A THESIS

FOR THE DEGREE OF MASTER OF ENGINEERING

Development of electrochemical capacitor using $NiCo_2O_4$ nanomaterials

TAE HYUN KIM

Department of Mechatronics Engineering

GRADUATE SCHOOL

JEJU NATIONAL UNIVERSITY

February –2017

Development of electrochemical capacitor using$NiCo_2O_4$ nanomaterials

TAE HYUN KIM

(Supervised by Professor Sang Jae Kim)

A thesis submitted in partial fulfillment of the requirement for the degree of Doctor of Philosophy

2016. 12

The thesis has been examined and approved.

Thesis Director, Prof. Lim Joung-Hwan	Professor, Department of Mechatronics Engineering, College of Engineering, Jeju National University
Thesis Committee Member, Prof. Kang Chul-ung	Professor, Department of Mechatronics Engineering, College of Engineering, Jeju National University
Thesis Committee Member, Prof. Sang-Jae Kim	Professor, Department of Mechatronics Engineering, College of Engineering, Jeju National University

December, 2016

Department of Mechatronics Engineering

GRADUATE SCHOOL

JEJU NATIONAL UNIVERSITY

REPUBLIC KOREA

CONTENTS

Nomenclature

BET	Brunauer-Emmet-Teller
CV	Cyclic voltammetry
DI	De-ionized
ECs	Electrochemical capacitors
EDLC	Electrochemical double layer capacitor
EES	Energy storage systems
EIS	Electrochemical Impedance spectroscopy
FE-SEM	Field-emission scanning electron microscopy
FT-IR	Fourier transform-infrared
GCD	Galvanostatic charge discharge
HK	Horvath-Kawazae
HT	Hydrothermal
JCPDS	Joint committee on powder diffraction standard
LEDs	Light emitting diodes
SCs	Supercapacitors
SCE	Saturated calomel electrode
XRD	X-ray diffraction
XPS	X-ray photo electron spectroscopy

List of Figures

초 록

현대 사회의 출현과 에너지의 수요 증가에 따른 화석 연료의 부족으로 인해 새로운 종류의 에너지 전환 및 저장 장치의 개발에 대한 관심이 높다. 에너지 저장 장치 중에서 슈퍼커패시터는 베터리를 대체 할 수 있는 저장 장치로 주목되어 왔다. 그러나 낮은 전기 용량 및 저 에너지 밀도를 갖는 물질로 인해 슈퍼커패시터 개발은 어려웠다. 본 학위 논문에서는 높은 페러데이 반응을 갖는 에너지 저장 장치용 전극인 이차 금속 산화물($NiCo_2O_4$)을 사용하였다. 첫 번째 실험에서는 쉬운 저온 수열 합성과 열적 어닐링 방법을 사용하여 $NiCo_2O_4$ 나노 플레이트를 제작했고 슈퍼커패시터에 적용했다. 제작 된 재료의 물리 화학적 특성을 X선 회절 분석, 푸리에변환 적외선 분광 분석(FTIR) 및 전계방출형 주사전자현미경(FE-SEM)을 통해 분석하였다. 그 결과 전기화학 측정에서 $NiCo_2O_4$ 나노플레이트 전극은 $5mVs^{-1}$의 스캔 속도에서 332 Fg^{-1}의 높은 비정전용량을 나타냈으며 $2.5Ag^{-1}$의 전류 밀도에서 2000 사이클의 후에도 초기 비정전용량의 약 86%을 유지함을 보여주었다. 두 번째 실험에서는 성능을 향상시키기 위해 니켈 폼 위에 견고한 접착력을 발휘하는 계층적 다공성 니켈-코발트 화형(porous hierarchical flower-shaped nickel, PFNC) 나노시트를 단순 수열 합성법 및 열처리를 통해 제작하였다. 재료 물질의 다공성 구조는 전기 활성을 증가 시키고 전기화학 측정을 하는 동안 빠른 전자 이동 및 이온 전도를 촉진시킨다. 제작 된 재료를 충•방전 분석 및 순환 전류 분석을 통해 측정한 결과 각각 5 $mAcm^{-2}$의 전류 밀도에서 최대 비정전용량은 2061 Fg^{-1}(표면정전용량 : $4.16Fcm^{-2}$)이고 5 mVs^{-1}의 스캔속도에서 최대 비정전용량은 $2100Fg^{-1}$($4.24Fcm^{-2}$)으로 측정되었다. 두 실험을 통해 바인더 물질이 혼합하지 않은 PFNC 전극이 슈퍼퍼캐시터 제작을 위한 좋은 양극 물질이 될 수 있음을 시사한다.

Abstract

The emergence of modern era and rising call for the need of energy urges the development of new kinds of energy conversion and storage devices due to lack of fossil fuels. Among the energy storage devices, supercapacitors have been considered as alternate energy storage devices for batteries. However, it suffers from low energy density due to the low capacitance materials. In the present thesis, we present a binary metal oxides, $NiCo_2O_4$ as an excellent electrode material for energy storage device due to its rich faradic reaction. In this first experimental, we present a preparation of $NiCo_2O_4$ nanoplates by a facile, low temperature, hydrothermal method, followed by thermal annealing and used supercapacitor applications. The physico-chemical characterizations of as-prepared materials were investigated by means of X- ray diffraction (XRD), Fourier transform infra-red spectroscopy (FT-IR) and field emission scanning electron microscopy (FE-SEM). The electrochemical measurements demonstrate that the $NiCo_2O_4$ nanoplates electrode exhibits a high specific capacitance of 332 F g^{-1} at a scan rate of 5 mV s^{-1} and also retained about 86% of the initial specific capacitance value even after 2000 cycles at a current density of 2.5 A g^{-1}. In order to improve the performance, we demonstrate a large-scale growth of porous hierarchical flower-shaped nickel cobaltite (PFNC) nanosheets on Ni foam with robust adhesion as a high performance electrode material for supercapacitors via a simple hydrothermal method and post annealing treatment. The presence of porous architecture increases the electroactive cites and facilitates the fast electron and ion conduction during

electrochemical measurements. The prepared material shows a maximum specific capacitance of 2061 Fg^{-1} (areal capacitance of 4.16 F cm^{-2}) at the current density of 5 mA cm^{-2} and 2100 F g^{-1} (4.24 F cm^{-2}) at the scan rate of 5 mV s^{-1} from charge discharge analysis and cyclic voltammetry analysis respectively. Overall results suggest that the prepared binder-less PFNC electrode will be a promising candidate as a positive electrode for supercapacitor applications.

Declaration

I, **Tae Hyun Kim**, hereby declare that the thesis entitled **"Development of electrochemical capacitor using $NiCo_2O_4$ nanomaterials"**, submitted to the Jeju National University, in partial fulfillment of the requirements for the award of the **Degree of Master of Engineering in Department of Mechatronics Engineering** is a record of original and independent research work done and published by me during the period March 2013 to February 2017 under the supervision and guidance of **Prof. Sang Jae Kim**, Department of Mechatronics Engineering, Jeju National University. This thesis solely based on our publication in reputed journals, and it has not been formed on the basis from the award of any other Degree / Diploma / Associateship / Fellowship.

Tae Hyun Kim

1. Introduction

1.1. Background

In recent years, the rapid growth of global economy, the depletion of fossil fuels and increasing environmental pollution stimulates the development of an efficient, clean and sustainable energy storage technology [1-3]. It is further found that this deficiency will be increased as double by the middle of this 21st century and this demand further will be increased as triple by the end of this 21stcentury. Presently, majority of the electricity demand is achieved by the generation of power from various non-renewable energy resources like crude oil, natural gas, coal, and nuclear energy. However, diminishing the availability of fossil fuels and raising the amount of greenhouse gas emissions made us urgent the society to take action towards renewable and sustainable energy resources. Particularly, wind and solar power are the most plentiful and abundant renewable energy resources than the any other resources such as bio-fuel, biomass, geothermal energy, etc. Although, the major obstacles of solar and wind power are, they could be produced only during daytime and wind does not blow on request respectively.

This variable nature of solar and wind resources leads to the origin and development of electrical energy storage (EES) systems. In this regard, electrochemical energy storage systems play an important role in storing electrical charge by converting the chemical energy into electrical energy and vice versa. The electrochemical energy storage systems has captivated among all other classes of EES due to its various

advantages such as high direct energy conversion, efficiency of energy conversion, non-appearance of mobile parts and hence portability, minimum noise level, miniaturization, convenient to scale up in large and minimum pollution [4, 5].

1.2.Energy storage devices

EES are extensively used in grid storage, UPS, electronic devices such as laptops, cell phones, digital cameras, power tools etc. In specific, the EES devices are widely employed in the expansion of electric or hybrid electric vehicles with less CO_2 emissions. The EES are largely categorized into three main types such as (i) batteries, (ii) capacitors and (iii) fuel cells. Capacitors are the device which storing the charge between the positive and negative electrodes which is separated by a dielectric medium. The capacitor is mainly analyzed using the term, capacitance. Generally, the output of dielectric capacitors is between several micros to several milli-farads. Capacitance is directly proportional to the surface are of the electrode materials and inversely proportional to the distance between the two electrodes. Supercapacitors are also called as, ultracapacitors, double-layer capacitors, electrochemical capacitors, power capacitors, gold capacitors and power cache.

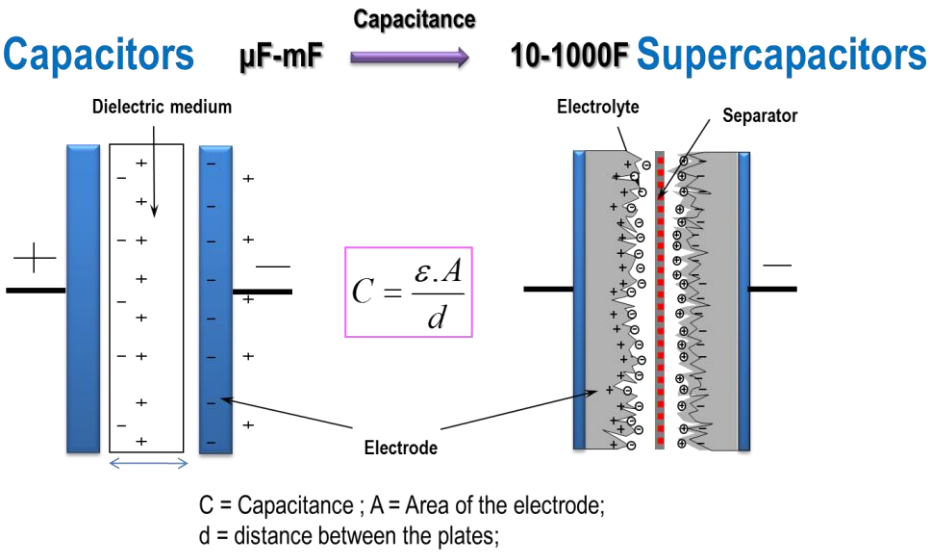

Figure. 1.1.1. Schematic representation of capacitors and supercapacitors

The EES charge storage mechanism is either by ion adsorption/desorption (electrical double layer capacitors) or redox reactions (pseudocapacitors). Thus, the storing of electrical charge is high in electrochemical capacitors than electrolytic and electrostatic capacitors. Moreover, supercapacitor has high power density than batteries and high energy density than conventional capacitors.

1.3. Types of electrochemical capacitors

Among the various energy storage technologies; supercapacitors have attracted an immense attention for the future generation devices, most importantly because of their fast charge/discharge process, high- power density, long cycle life and environmentally benign [6-9].Therefore, they are extensively utilized in electric vehicles, portable

electronics, and memory back-up systems [10]. Supercapacitors are popularly categorized into electric double layer capacitors (EDLCs) and pseudocapacitors based on their charge storage mechanisms [2, 3, 10, and 11].

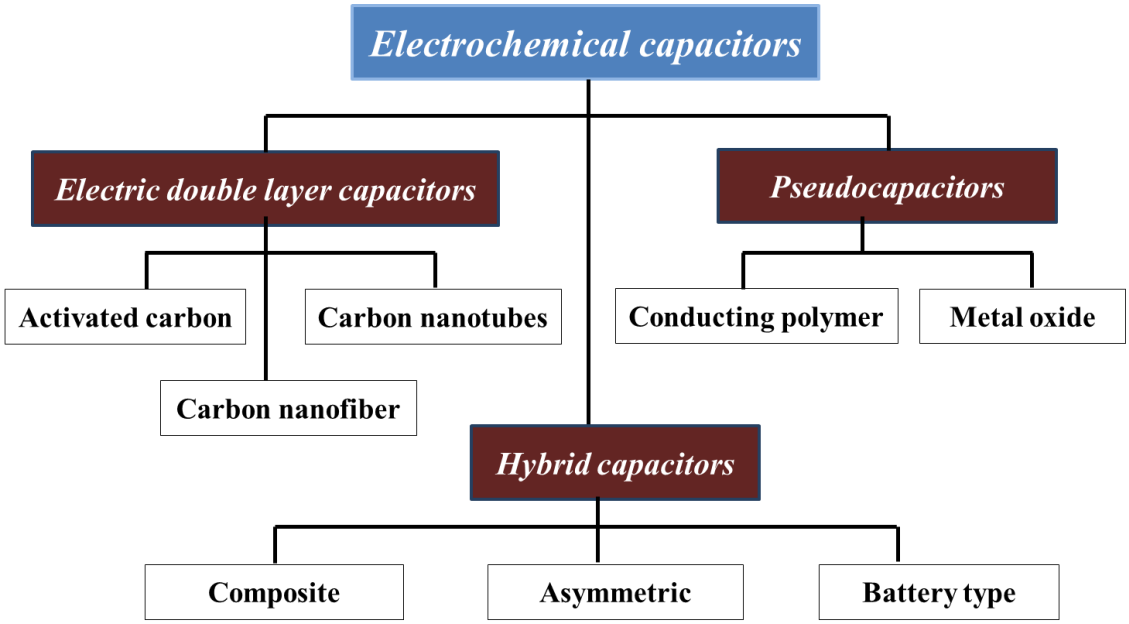

Figure.1.1.2. Chart for types of supercapacitors

1.3.1. Electrical double layer capacitors (EDLC)

In (EDLCs), the capacitance is mainly correlated with the gathering of charge at the interface between electrode and electrolyte as double layer, called as non-Faradaic process. Although, the amount of charge accumulation is investigated by using the following equation to that of parallel-plate capacitor, $C = \varepsilon.S/d$, therefore, Where, $\varepsilon = \varepsilon_o.\varepsilon_r$, ε_o is the permittivity of free space (8.854×10^{-12} F m^{-1}) and ε_r the relative dielectric constant of the electrolyte as liquid or solid, A is the surface area of the electrodes (m^2 g^-

[1]) and d is the thickness of the electrical double-layer (EDL) or Debye length. The famous scientist Helmholtz was firstly proposed the model for EDL theory in 1853 likewise to that of parallel plate capacitor; hence this model tells that two layers of opposite charges build up at the interface between electrode-electrolyte with little atomic distance. Carbon based materials are the best examples for double layer capacitors such as activated carbon, carbon nanotubes and graphene and so on, have been used to store charges in EDLCs.

1.3.2. Pseudocapacitors

The electrochemical performance of supercapacitor is mainly based on their electrode material's property [3]. Till now, the practical application of supercapacitors are hindered due to insufficient performance of the electrode materials, such as low specific capacitance of carbon-based materials, high cost (RuO_2), poor electrical conductivity and poor cycling stability of transition metal oxides [12]. Therefore, significant research efforts have been devoted to improve the electrochemical performance of electrode materials for high-performance supercapacitors and it is one of hot research topic this field. Transition metal oxides have many intriguing properties with numerous oxidation states which capable of enhanced redox reactions resulting to achieve excellent electrochemical output than the conventional carbon based materials and conducting polymers [13-15]. This interesting behavior makes the transition metal oxides as the potential electrode materials for supercapacitor applications. There are

much efforts has been considered to developing a new disguised electrode materials with abundant nature, biocompatibility, low cost, eco-friendly nature and enhanced electrochemical performances such as MnO_2, NiO, Co_3O_4, $Ni(OH)_2$, $Co(OH)_2$ and so on [16-20]. However, due to slight increased semi-conducting nature, these materials have less transport between electrolyte and electroactive materials. Hence, it is necessary to find out an alternate advanced electrode material with excellent output. Recently, various kinds of inexpensive binary/ternary metal oxide systems such as Ni-Mn oxide [21], Mn-Co oxide [22, 23], Ni-Co oxide [24], Mn-Fe oxide [25], Ni-Ti oxide [26], Sn-Al oxide [27], Mn-Ni-Co oxide [28], Co-Ni-Cu oxide [29] and Mn-Ni-Cu oxide [30] have been put forward as the electrode materials for high-performance supercapacitors application due to their combined redox contribution of both metal ions. Therefore, it is significant and challenging to exploit multicomponent metal oxide materials for supercapacitors.

Among them, $NiCo_2O_4$ is an alternate promising material due to its high theoretical capacity, natural abundance, environmentally benign and low cost. Currently, spinel nickel cobaltite ($NiCo_2O_4$) has drawn an increasing attention as a promising electrode material for high-performance supercapacitors due to their high theoretical capacitance, low cost, environmental friendliness and natural abundance [31-37]. In addition to that, $NiCo_2O_4$possesses much better electrical conductivity, at least two orders of magnitude higher and better electrochemical activity than that of nickel oxide (NiO) and cobalt oxide (Co_3O_4) [38, 39]. So far, a various forms of

$NiCo_2O_4$nanostructures, including nanosheets, nanowires, nanoflowers, microspheres, and nanoplates have been synthesized and investigated for their electrochemical performances [40-44]. All these results demonstrate that the electrochemical properties of the electrode materials are highly related to their size, shape and morphology [45-47]. Therefore, it is necessary to develop a facile, scalable and low cost method to synthesize high-performance nanostructure materials with desirable morphology and size for supercapacitor applications. In recent years, there are many reports are available by using $NiCo_2O_4$ as an electrode material for supercapacitors such as nanoflakes, nanoparticles, nanoneedles, nanoflowers, nanowires, nanorods and so on with and without additive agent. On the other hand, creating the three dimensional hierarchical nanostructures materials have been considered much attention in the recent days making them to improve ion transportation in energy storage devices [48, 49]. In addition developing porous structures materials will improve the exposed specific surface area of the electrode materials which leads to better specific capacitances.

1.4.Scope of this present thesis

The literature review portrays that the binary metal oxide, especially $NiCo_2O_4$nanomaterialsare one of the prominent electrode materials for the high performance supercapacitor and their specific capacitance value is mainly depends on the synthesis and morphology of the material. Thus, it is important to find out the suitable synthesis procedure and new fabrication technique to prepare $NiCo_2O_4$ for electrochemical energy storage devices. The main scope of this thesis are described as follows,

- To synthesize plate-like structure of $NiCo_2O_4$as non-binder-free electrode and Porous flower-like $NiCo_2O_4$ nanosheets on Ni foam as binder-free electrode by facile hydrothermal method for supercapacitors
- To investigate the structural characteristics of the prepared materials by Field-emission scanning electron microscopy (FE-SEM), N_2 adsorption / desorption, X-ray diffraction (XRD), X-ray photoelectron spectroscopy (XPS) and Fourier transform Infrared spectroscopy (FT-IR)
- To elucidate the electrochemical characteristics of the prepared electrodes using cyclic voltammetry (CV), electrochemical impedance spectroscopy (EIS) and galvanostatic charge-discharge (GCD) techniques

The results demonstrated in this thesis may benefit simple and effective approaches to preparing transition binary metal oxide and their improved

electrochemical performances via binder-free approaches as electrode materials for electrochemical energy storage systems.

2. Materials and methods

2.1.Chemicals

All the chemicals used in this thesis were of research grade and directly used without any further purification. The list of chemicals used in this thesis is given in **Table2.1.**

Table 2.1 Chemicals used in this thesis work.

Chemicals	Formula	Purity	Supplier
Nickel nitrate hexahydrate	$Co(NO_3)_2.6H_2O$	97%	Daejung Chemicals & Metals Co. Ltd, Korea
Nickel chloride hexahydrate	$CoCl_2.6H_2O$	97%	Daejung Chemicals & Metals Co. Ltd, Korea
Cobalt nitrate hexahydrate	$Co(NO_3)_2.6H_2O$	97%	Daejung Chemicals & Metals Co. Ltd, Korea
Cobalt chloride hexahydrate	$CoCl_2.6H_2O$	97%	Daejung Chemicals & Metals Co. Ltd, Korea
Hydrochloric acid	HCl	35%	Daejung Chemicals & Metals Co. Ltd, Korea
Potassium hydroxide	KOH	85%	Daejung Chemicals & Metals Co. Ltd, Korea
Polyvinylidene fluoride (PVDF)	$(CH_2CF_2)n$	-	Sigma Aldrich
Carbon black	C	99%	Sigma Aldrich
N-Methyl-2-pyrrolidinone (NMP)	C_5H_9NO	99.7%	Daejung Chemicals & Metals Co. Ltd, Korea
Ethanol	CH_3CH_2OH	99.9%	Fisher Scientific
Acetone	C_3H_6O	99.8%	Fisher Scientific

Sulfuric acid	H_2SO_4	98%	Daejung Chemicals & Metals Co. Ltd, Korea
Sodium hydroxide	NaOH	98%	Daejung Chemicals & Metals Co. Ltd, Korea
Potassium hydroxide	NaOH	98%	Daejung Chemicals & Metals Co. Ltd, Korea
Poly(tetrafluoroethylene) (PTFE)	$(C_2F_4)_n$	-	Sigma Aldrich
Nickel foam	Ni	-	Heze Jiaotong Group Corporation, China
Nitric acid	(HNO_3)	60-62%	Junsei Chemical Co. Ltd. Japan

2.2. Synthesis procedure

2.2.1. Hydrothermal synthesis

Hydrothermal method is one of the good techniques that have numerous benefits, such as facile, lower cost, eco-friendly, able to prepare with excellent morphology, and the feasibility of gaining improved accessible active sites. Hydrothermal process has considered as one of the potential approaches for preparing nanomaterials with different morphologies. Hydrothermal technique is a method that uses homo- or heterogeneous phase reactions in aqueous medium at the high pressure above 1 atm and high temperature above 100 ℃ to crystallize nanomaterials from precursor solution [50, 51]. At the sealed steel vessel of autoclave, the growth process was performed that can sustain in high pressures and temperatures for a long time along with water. A temperature incline was preserved inside the reaction chamber between the two opposite ends. At the side of hotter end, the precursor solute dissolves, whereas at the side of

cooler end, it is deposited as a seed crystal, which leads to growing the desired crystal. The hydrothermal method was used to prepare the electrode materials as presented in this thesis.

2.3. Materials characterization

2.3.1. X-ray diffraction technique (XRD)

X-ray diffractometer (XRD) is one of the non-destructive methods to determine the phase of the crystal, crystal size, phase purity, and structure. The prepared samples were performed by using Rigaku X-ray diffractometer which is operated with Cuk_{α} radiation at 40 KeV and 40 mA in the range between10 and 80° with a step range of 0.02°.

2.3.2. Fourier transform infrared (FT-IR) spectrometer

The functional groups presented in the samples were analyzed using FT-IR spectroscopy. FT-IR spectra were measured using Thermo Scientific Systems, Nicolet-6700 at room temperature using the KBr pellet method in the range between 4000 and 400 cm^{-1}.

2.3.3. Field-emission scanning electron microscopy

The morphology of the desired surface and size of the particles of the synthesized materials were evaluated using the field-emission scanning electron (Model: FE-SEM, JSM-6700F, JEOL Ltd) with filament current of 10 μA and an acceleration voltage of 5 kV. Prior to measurement, the prepared samples were affixed onto a double-

face conducted tape mounted on a metal stud and coated with platinum using a sputter coater (model: Cressing ton sputter coater -108 auto).

2.3.4. X-ray photoelectron spectroscopy (XPS)

The chemical state of elements and compositions present in the surface of the samples was obtained by XPS technique using model: ESCA- 2000, VG Microtech Ltd and Theta Probe AR-XPS system (Thermo Fisher Scientific, U.K). In this, a monochromatic X-ray beam source was used at 1486.6 eV (using aluminum anode) and 14 kV was used to scan over the surface of the prepared sample.

2.3.5. Brunauer, Emmett and Teller (BET) surface area analysis

BET surface area analysis, also called as Nitrogen (N_2) adsorption-desorption isotherm is one of the important techniques measurement was carried out to determine the pore-volume and pore-size and especially specific surface area, as-prepared samples. The BET analysis was performed with Quantachrome RASiQwin™ c 1994-2012, Quantachrome Instruments v2.02 and nitrogen (N_2) gas was used as an adsorptive for the determination of the above parameters. The multiple-point model was used to calculate the specific surface area. The Horvath-Kawazae (HK) method was used to measure pore size distributions which is obtained from the adsorption/ desorption. The total pore volume was calculated from the volume of nitrogen adsorbed at a relative pressure of P/Po =0.95.

2.4. Electrochemical Testing

2.4.1. Cyclic voltammetry (CV)

CV is commonly considered as an appropriate technique tool for evaluating the difference between the EDLC and faradaic behavior in an electrochemical reaction. In CV measurement, the voltage is sweeping from a lower limit to an upper limit at a fixed voltage. The slope of the line is used to calculate the voltage scan rate. The evolution of current was measured as voltage function. The CV data of the prepared non binder-free and binder-free electrodes were obtained by increasing the scan rates like 2, 5, 10, 25, 50, 75, and 100 mV s^{-1}.

2.4.2. Galvanostatic charge/discharge

The galvanostatic charge/discharge (GCD) studies are the most important and direct approach to evaluate the applicability of supercapacitors. A repetitive curve of charge and discharge analysis is called as a cycle. Mostly, at the constant current, the charge and discharge are conducted upto a set potential is reached. The galvanostatic charge/discharge curves of the prepared non binder-free and binder-free electrodes were obtained for different current densities.

2.4.3. Electrochemical impedance spectroscopy (EIS)

EIS is a powerful technique to understand the capacitive behavior and impedance attributed with the fabricated electrode surface. This creates the feasibility for further electrochemical measurements. EIS is the most general method for evaluating the equivalent series resistance (ESR) of the electrode material. It further permits producing the models to define, underlying reaction mechanisms.

3. Synthesis and characterization of $NiCo_2O_4$ nanoplates as efficient electrode materials for electrochemical supercapacitors

Highlights

- In the present work, $NiCo_2O_4$ nanoplates were prepared by a facile, low temperature, hydrothermal method, followed by thermal annealing and used supercapacitor applications.
- The physico-chemical characterization of as-prepared materials was studied by using X-ray diffraction (XRD) spectroscopy, Fourier transform infra-red (FT-IR) and field emission scanning electron microscopy (FE-SEM).
- The electrochemical measurements demonstrate that the $NiCo_2O_4$ nanoplates electrode (NC-5) exhibits a high specific capacitance of 332 F g^{-1} at a scan rate of 5 mV s−1and also retained about 86% of the initial specific capacitance value even after 2000 cycles at a constant current density of 2.5 A g^{-1}.
- These results suggest that the fabricated electrode material has huge potential as a novel electrode material for electrochemical capacitors.

3.1. Experimental section

3.1.1. Synthesis of $NiCo_2O_4$

All the chemicals used in this experiments were analytical grade and used without further purification. $NiCo_2O_4$ nanoplates were synthesized via a hydrothermal process (**Scheme. 3.1.1**).

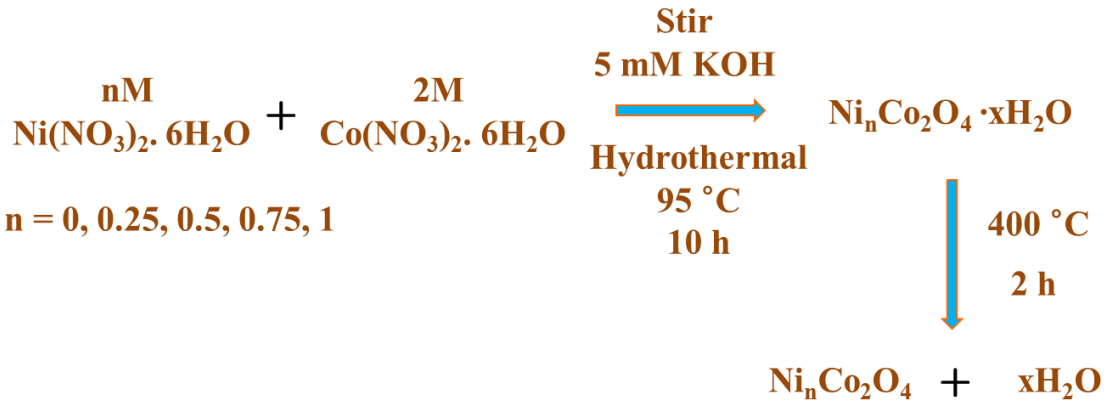

Scheme.3.1.1. Representation of synthesis of $NiCo_2O_4$

In a typical experiment, the different molar ratio of cobalt nitrate ($Co(NO_3)_2$), and nickel nitrate ($Ni(NO_3)_2$) were dissolved in 100 mL of deionized water with continuous stirring for 30 min. Followed, 5 mM of potassium hydroxide (KOH) was added drop wise to the above solution and stirred for 15 min at room temperature. Then the solution was transferred in to the Teflon-lined stainless steel autoclave (100 ml capacity), sealed and then heated to 95 ℃ for 10 h. After cooling down to room temperature naturally, the precipitate was collected and washed with deionized water and then dried in air at 60 ℃ for overnight. Finally, the as-prepared samples were calcined at 400 ℃ for 2 h in air to

obtain the $NiCo_2O_4$ In this study, five samples were prepared by varying the molar ratio of $Ni(NO_3)_2$ (i.e., 0, 0.25, 0.5, 0.75 and 1 M). The final samples were denoted as NC-1, NC-2, NC-3, NC-4 and NC-5, respectively.

3.1.2. Electrochemical Analysis

The working electrodes were prepared by manual slurry coating technique as follows; 80 wt% of active materials ($NiCo_2O_4$), 10 wt% of acetylene black, 10 wt% of polyvinylidene fluoride (PVDF) binder were mixed together with a small amount of NMP to produce a homogeneous paste, which was coated onto the nickel foam current collector (1x1 cm^2). The prepared electrodes were dried in a vacuum drying oven at 120 ℃ for 24 h. The electrochemical measurements cyclic voltammetry, galvanostatic charge- discharge and electrochemical impedance were performed in 2 M KOH solution in a three-electrode cell using an Autolab PGSTAT302N electrochemical work station. Platinum foil as counter and an Ag/AgCl as reference electrodes were used.

3.2.Results and discussion

$NiCo_2O_4$ nanoplates were prepared by a facile hydrothermal method using cobalt nitrate and nickel nitrate precursors at 95 ℃ for 10 h and then further calcined at 400 ℃ for 2 h. The structural, morphological and electrochemical properties of the as-prepared samples were discussed in detail as follows.

The crystal structure and purity of the as-prepared samples were analyzed using XRD. **Figure. 3.1.1** shows the typical XRD patterns of NC-x (x= 1, 2, 3, 4 and 5) samples. The XRD pattern of Co_3O_4 could be indexed to the cubic phase (JCPDS No.

65-3103) and also the $NiCo_2O_4$ (NC-x; x = 2, 3, 4 and 5) revealed the cubic structure. It could be seen that all of the identified peaks are consistent with the standard pattern (JCPDS No. 73-1702) of cubic $NiCo_2O_4$ with spinel structure [39]. No other diffraction peaks were observed, which confirms the phase purity of $NiCo_2O_4$ nanoplates.

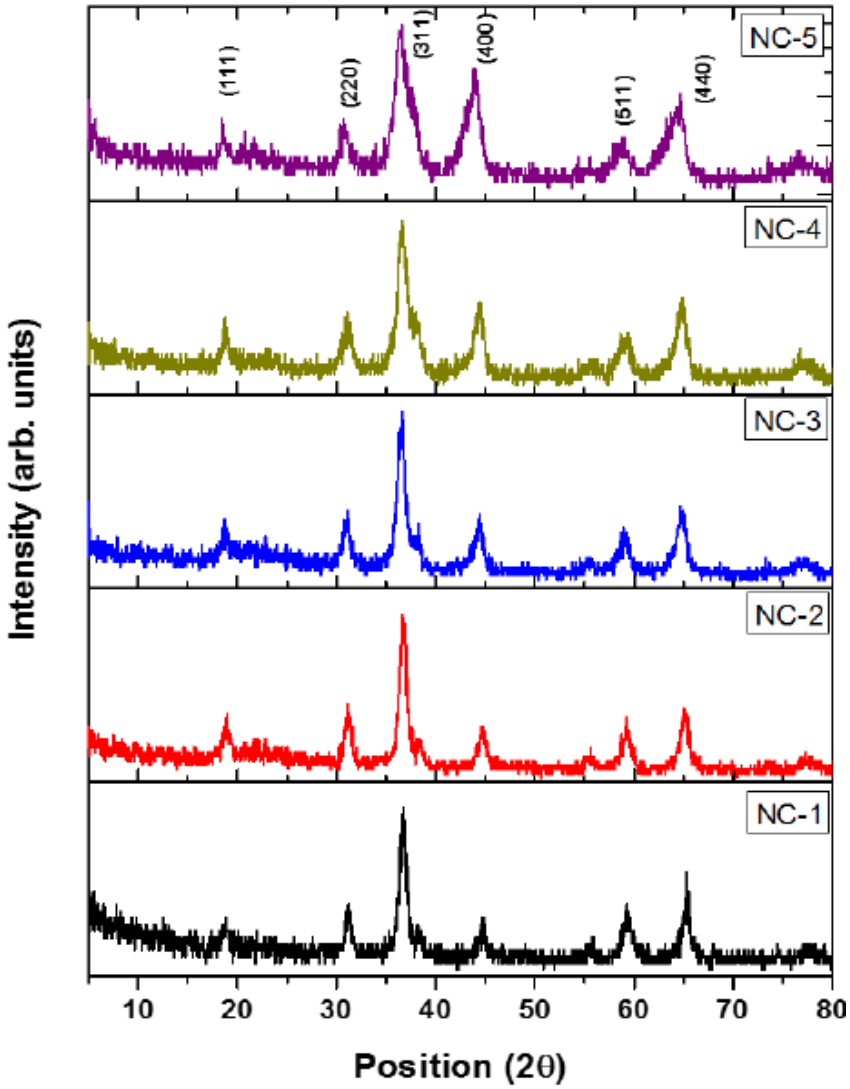

Figure.3.1.1 XRD patterns of (a) NC-1, (b) NC-2, (c) NC-3. (d) NC-4, and (e) NC-5 sample.

Further, with increasing the molar ratio of nickel ions in the spinel structure, the diffraction peaks become broadening, which indicates that the crystallite sizes of the as-prepared samples are in nanometer range.

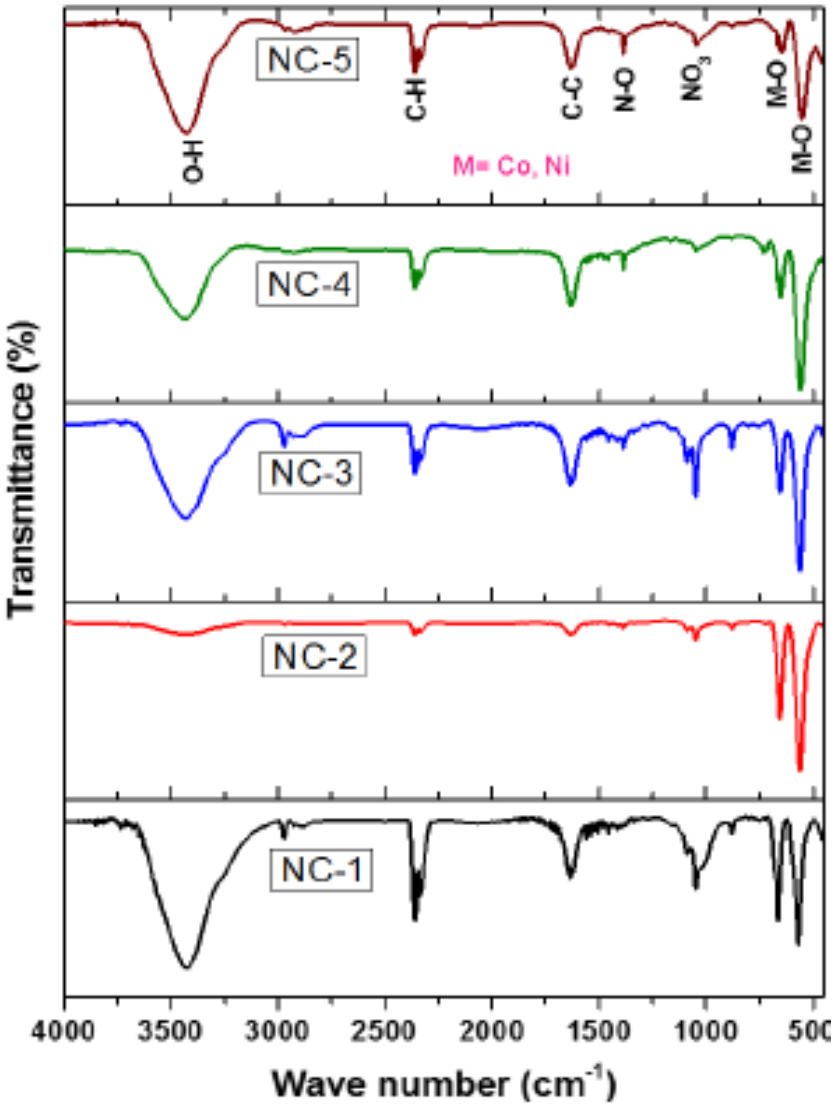

Figure.3.1.2. FTIR spectra of (a) NC-1, (b) NC-2, (c) NC-3. (d) NC-4, and (e) NC-5 sample.

The FT-IR spectra of $NiCo_2O_4$ nanoplates (NC-1, NC-2, NC-3, NC-4 and NC-5) are shown in **Figure. 3.1.2.** The peak observed at 3440 cm^{-1} in all spectra is assigned to the stretching vibration of O-H group in water molecules. The two bands appeared at 2349, and 1622 cm^{-1} are due to the C-H, and C=C vibrations. The absorption bands at 1377 cm^{-1} associated with the symmetric stretching vibration of N-O bond and the band at 1049 cm^{-1}corresponded to N-O stretching vibration from the NO_3group. The lower frequency peaks at 650 and 538 cm^{-1}can be assigned to the stretching vibrations of the metal oxygen bonds in $NiCo_2O_4$ [52, 53].

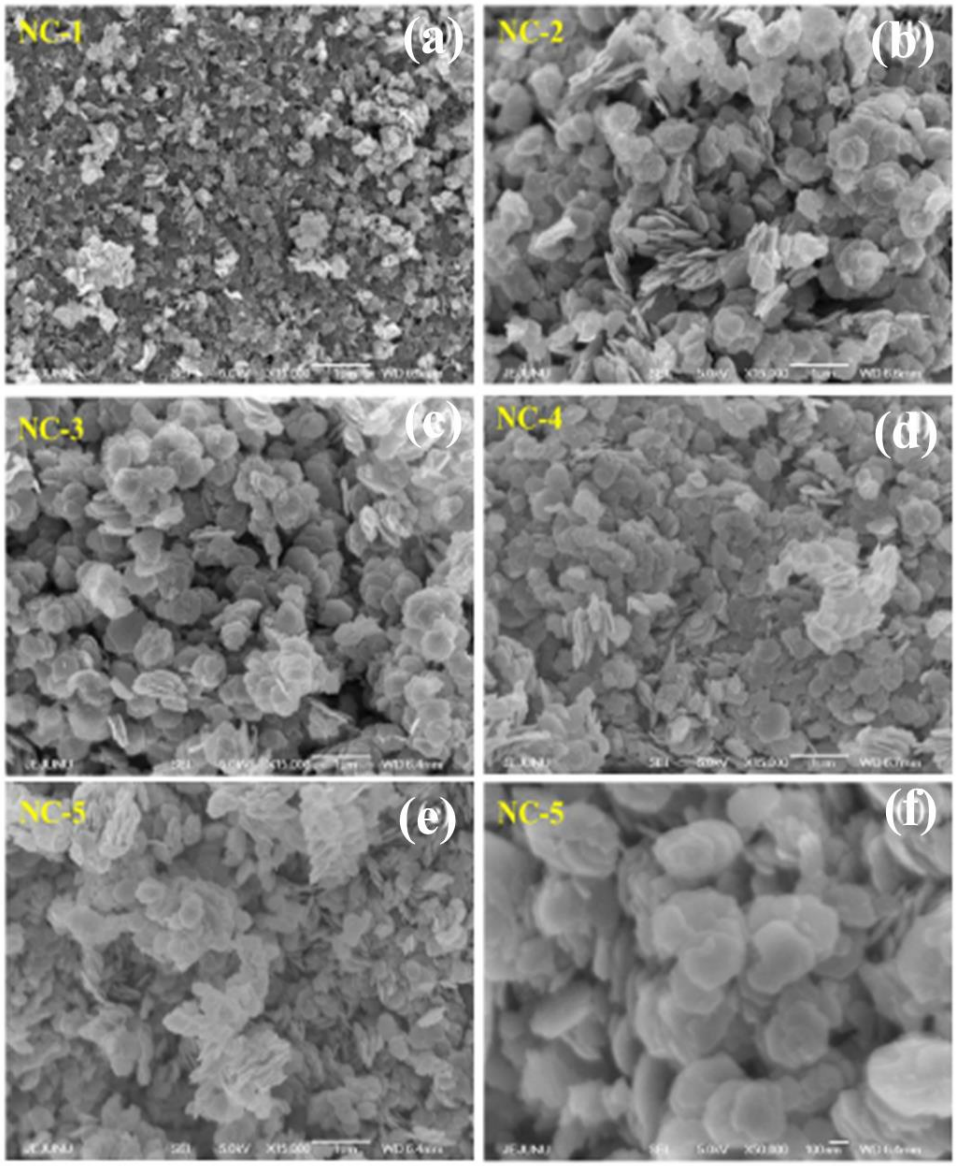

Figure. 3.1.3. FE-SEM images of (a) NC-1, (b) NC-2, (C) NC-3, (d) NC-4, (e-f) NC-5

Figure 3.1.3 shows the typical FE-SEM images of NC-1, NC-2, NC-3, NC-4, and NC-5 samples. It can be clearly seen that the Co_3O_4 (**Figure 3.1.3 (a);** NC-1) and $NiCo_2O_4$ images (**Figure 3.1.3 (b-e);** NC-2, NC-3, NC-4, and NC-5) exhibit the platelet

structure with a diameter of 200 to 300 nm and the thickness of about 25 nm. Further, the high magnification image of $NiCo_2O_4$ (Figure 3.1.3. (f)**)** nanoplates reveal the existence of many pores in the nanoplates.

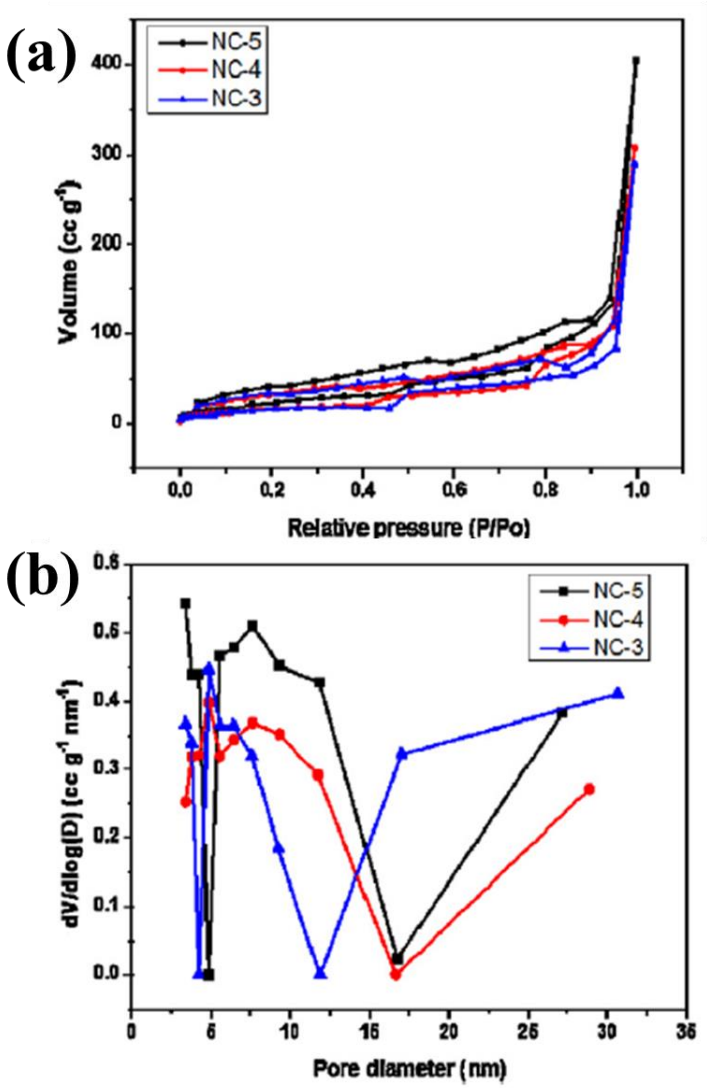

Figure.3.1.4. (a) N_2 adsorption/desorption isotherms and (b) pore-size distribution curves of the NC-3, NC-4 and NC-5 samples.

Nitrogen (N_2) adsorption-desorption isotherm measurements were further performed to investigate the specific surface area and pore-size distribution of the selected NC-3, NC-4 and NC-5 samples. The N_2 adsorption-desorption isotherm and Barrett-Joyner-Halenda pore-size distribution plots for the NC-3, NC-4 and NC-5 samples are shown in **Figure. 3.1.4 (a, b)**. It could be observed that all the samples exhibited a hysteresis loop and the BET specific surface area was calculated to be 53.4 (NC-3), 56.9 (NC-4), and 83.8 m^2 g^{-1} (NC-5). The corresponding pore-distribution was calculated by the BJH method, which is shown in **Figure 3.1.4. b**. The average pore size distribution and the pore volume of the NC-3, NC-4 and NC-5 samples were calculated to be 3.4, 3.7, and 3.3 nm and 0.44, 0.45, and 0.59 cc g^{-1}, respectively. These results confirm that the NC-5 sample exhibits the high surface area, large pore volume and well-formed meso-porosity, which facilitates more electroactive sites for electrochemical reactions (energy storage).

The capacitance behavior of as-prepared $NiCo_2O_4$ nanoplates electrodes were examined by electrochemical impedance spectroscopy, cyclic voltammetry, galvanostatic charge-discharge techniques in 2 M KOH electrolyte solution. **Figure.3.1.5 (a)** displays the Nyquist plots of $NiCo_2O_4$ nanoplates electrodes (NC-2, NC-3, NC-4 and NC-5). The inset of Figure 5a shows the Nyquist plot of NC-1 electrode. Almost all the plots showed the semi-circle arc at high-frequency region and followed by a straight line in the low-frequency region [54]. The semi-circle arc at the high-frequency region indicates that the charge transfer resistance (Rct) occurs at the

electrode/electrolyte interface [55]. Further, the 45° incline line of the Nyquist plots (low frequency region), demonstrates a Warburg type impedance of the electrolyte ions into the interior portion (bulk) of the electrode [56]. Compared to the Co_2O_3 (inset **Figure 3.1.5 (a)** NC-1) electrode, the $NiCo_2O_4$ electrodes possessed smallest semi-circle arc, demonstrates the best electrochemical conductivity. These results suggest that as-prepared $NiCo_2O_4$ electrode materials have better electrical conductivity.

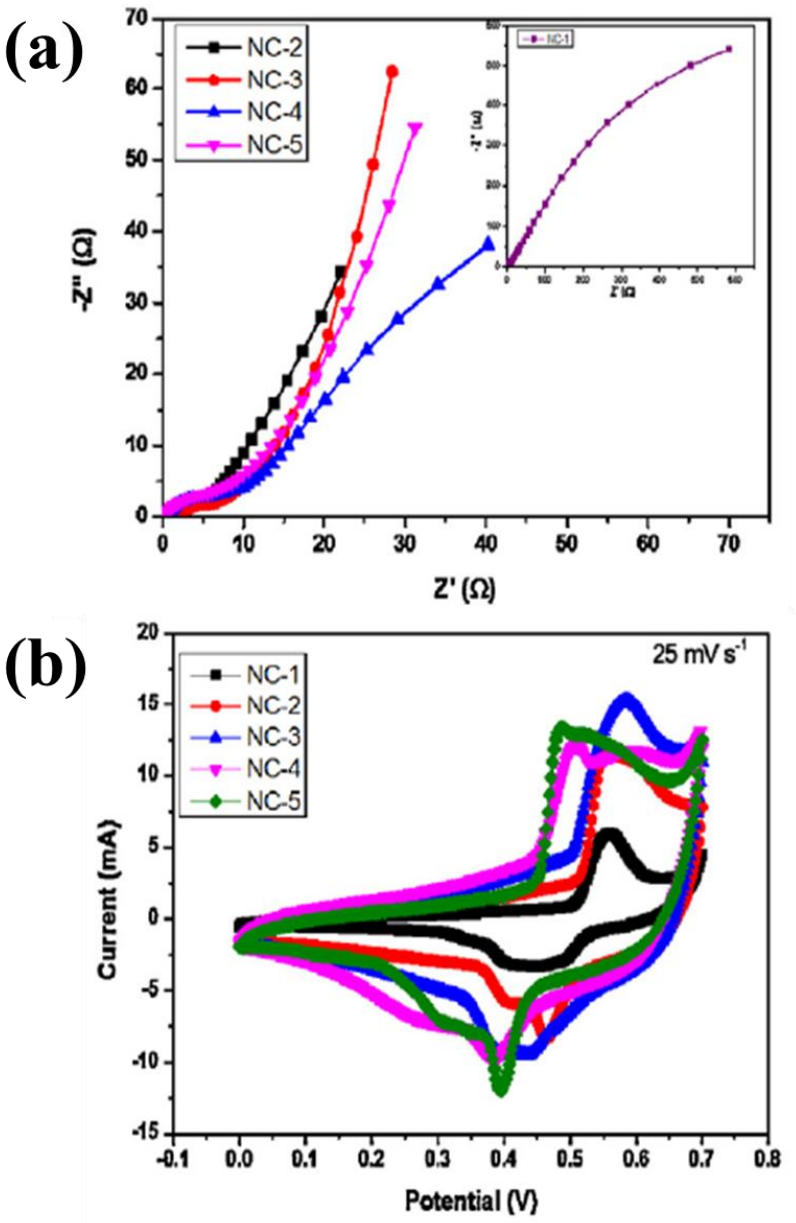

Figure.3.1.5.(a) EIS spectra of NC-2, NC-3, NC-4 and NC-5 electrodes; the inset is the Nyquist plot of NC-1. (b) CV plots of NC-1, NC-2, NC-3, NC-4 and NC-5 electrodes at the scan rate of 25 mV s^{-1}.

The CV curves of NC-1, NC-2, NC-3, NC-4 and NC-5 electrodes at a scan rate

of 25 mV s^{-1}, shown in **Figure. 3.1.5 (b)**. It can be noticed that the CV curve displays two oxidation peaks in the anodic process and two reduction peaks in the cathodic process, which confirms that the capacitive behavior of the electrode is mainly governed by faradaic reaction. The two sets of redox peaks were related to the reversible reactions of Ni^{2}+/Ni^{3}+ and Co^{2}+/Co^{3}+ transitions. The redox reactions of $NiCo_2O_4$ in the alkaline (KOH) electrolyte are based on the following equations [57-59].

$$NiCo_2O_4 + OH^- + H_2O \longleftrightarrow NiOOH + 2CoOOH + 2e^- \quad \text{..... (3.1)}$$

$$CoOOH + OH^- \longleftrightarrow CoO_2 + H_2O + e^- \quad \text{..... (3.2)}$$

Compared to NC-1, the $NiCo_2O_4$ nanoplates electrodes showed increased redox current density, which suggests that $NiCo_2O_4$ nanoplates electrode have improved electrochemical performance. In particular, NC-5 electrode showed the larger integrated areas, among the $NiCo_2O_4$ electrodes. These result confirmed that the electrochemical properties of $NiCo_2O_4$ can be improved by the addition of a suitable of amount of nickel ions into the cobalt oxide matrix.

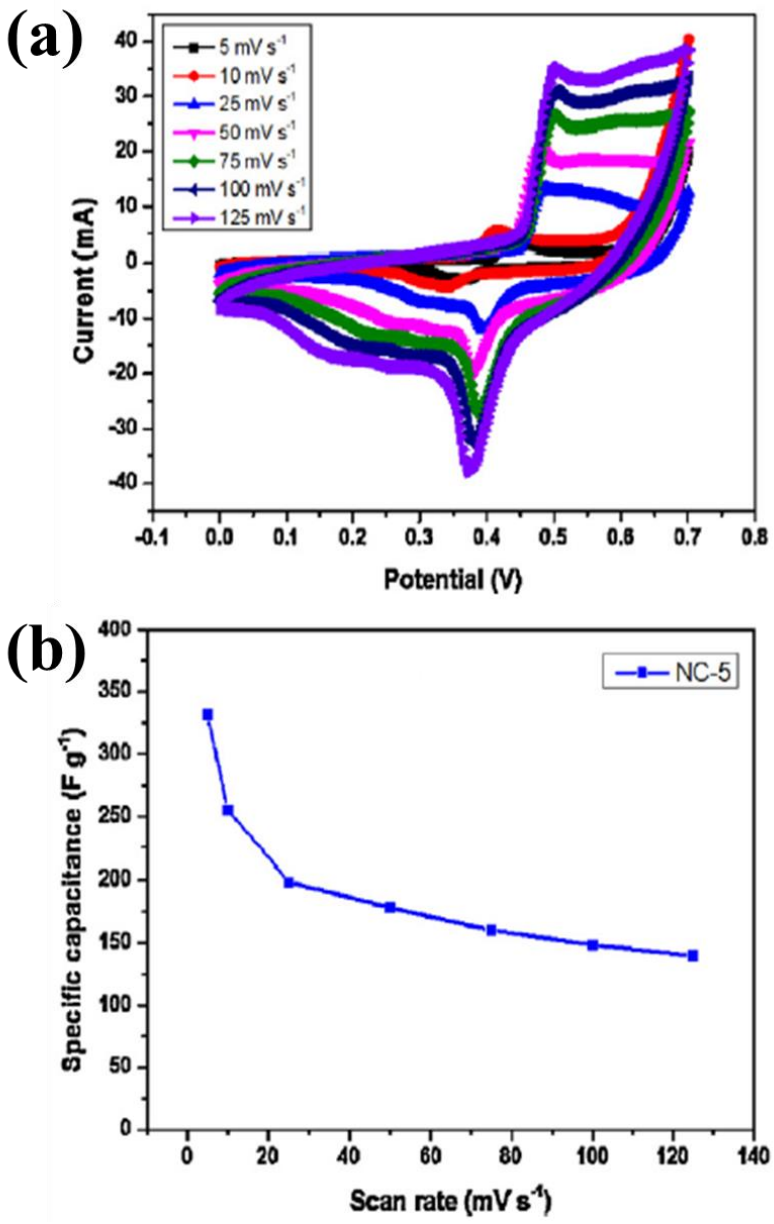

Figure. 3.1.6. (a) CV curves of the $NiCo_2O_4$nanoplates electrode (NC-5) at different scan rates. (b) Specific capacitance of the NC-5 electrode at different scan rates.

Furthermore, the detailed capacitance behavior of the NiCo2O4 electrode (NC-5)

was studied by CV measurements (**Figure. 3.1.6(a)**) with various sweep rates ranging from 5 to 125 mV s^{-1}. It is found that all the CV curves exhibited a similar shape, and a pair of well-defined redox peaks occurred during the cathodic and anodic process, which confirms the existence of pseudocapacitive characteristics. In addition, the scan rate rising from 5 to 125 mV s^{-1}, the position of the anodic and cathodic peaks slightly shifts to higher and lower potentials, respectively.

This phenomenon indicates that the quasi-reversible feature of the redox couples [60]. Further, the peak current increases noticeably with increasing scan rate that demonstrates the good rate capability and better pseudocapacitive behavior of the electrode material. The specific capacitance can be calculated using the following relation [61]

$$C = \frac{\int I \times dV}{v \times m \times \Delta V} \text{ ---------- (3.3)}$$

Where ∫Idv is the integral area under the CV curve (A), v is the scan rate (mV s^{-1}), m is the electroactive material (g), and AV is the potential window (V).The calculated specific capacitance of NC-1, NC-2, NC-3, NC-4 and NC-5 electrodes are 72, 200, 211, 237, and 332 F g^{-1} at a scan rate of 5 mV s^{-1}, respectively.

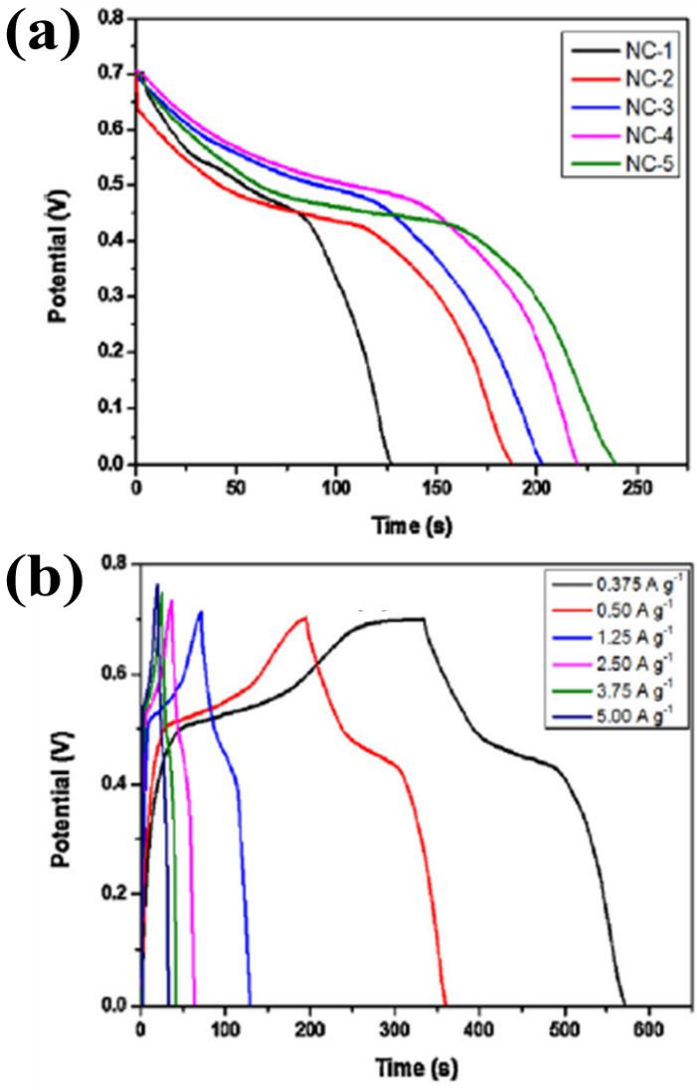

Figure.3.1.7. (a) Discharge curves **of NC-1, NC-2, NC-3, NC-4 and NC-5 electrodes at a current density of 0.375 A g^{-1}. (b)Galvanostatic charge-discharge curves of the $NiCo_2O_4$nanoplate electrode (NC-5) at various current densities in 2 M KOH**

Further, it is observed that the specific capacitance increases in the order of NC-1<NC-2<NC-3<NC-4<NC-5. The increase in specific capacitance is due to the suitable addition of Ni-ions into the **Co_3O_4** matrix. By introducing Ni-ions into the Co_3O_4 matrix,

the electrical conductivity of the $NiCo_2O_4$ could be enhanced and facilitate the fast ions transport between electrode and electrolyte interface, which leads to the higher specific capacitance [62, 63]. In addition to that, the enhanced electrochemical performance may be attributed to the increased surface area and porous structure, which provides the numerous active sites and more facile ion diffusion paths for the efficient charge storage. **Figure.3.1.6 (b)**shows the specific capacitance of NC-5 electrodes at different scan rates. While increasing scan rate, the specific capacitance decreases gradually, this is due to the active surface areas becoming inaccessible for charge storage at the higher scan rate.

Further the electrochemical performances of as-prepared electrodes were evaluated using galvanostatic charge/discharge test. **Figure. 3.1.7 (a)** shows the discharge curves of NC-1, NC-2, NC-3, NC-4 and NC-5 electrodes obtained at a constant current density of 0.375 A g^{-1}. It can be seen that all the discharge curves exhibits a similar shape. In addition, there are voltage plateaus in the discharge process and these plateaus are consistent (match well) with the results obtained from CV curves. This phenomenon indicates that the as-prepared samples exhibit a pseudocapacitance behavior, which is caused by a charge transfer reaction at the electrode/electrolyte interface. Compared with Co_3O_4, the $NiCo_2O_4$ electrodes showed higher discharge time at the same current density. This indicates that $NiCo_2O_4$ electrodes have higher charge storage capacity than that of the Co_3O_4 electrode.

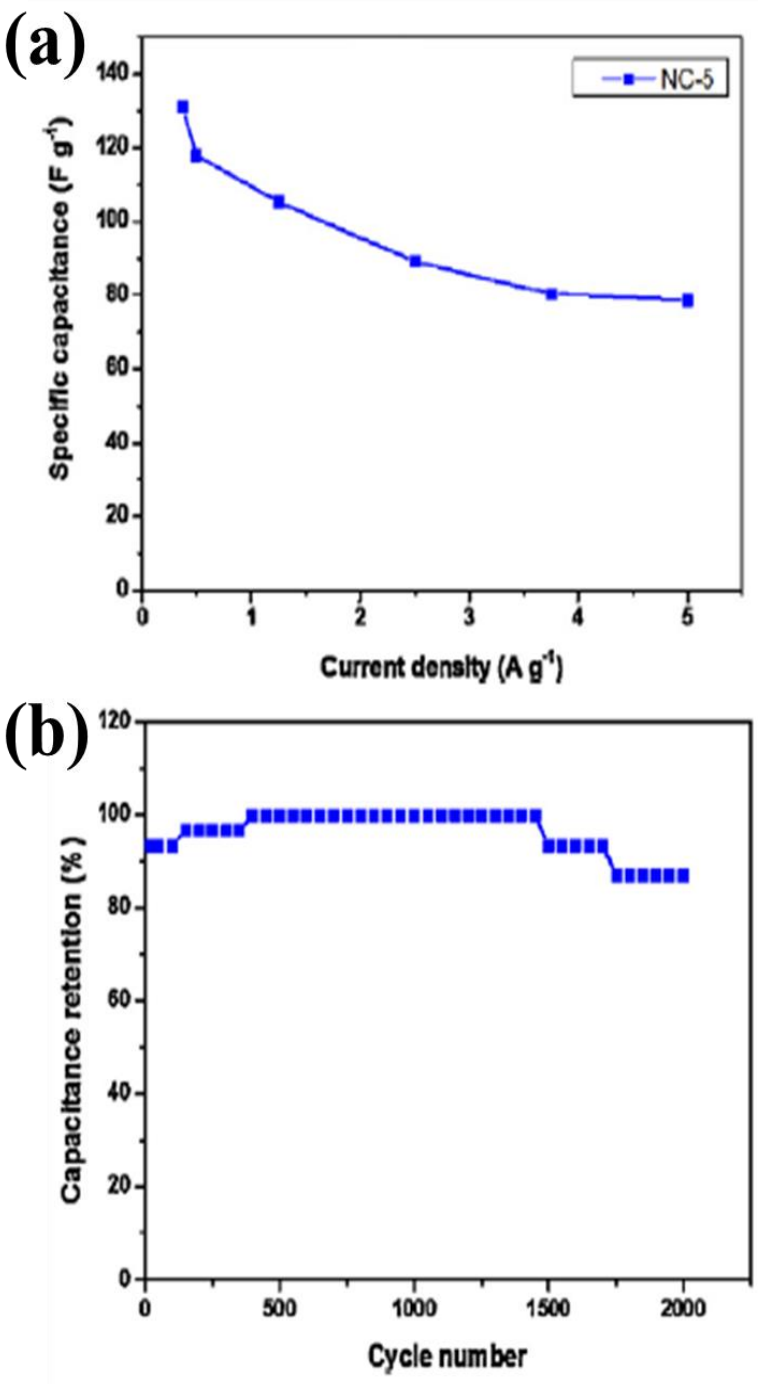

Figure. 3.1.8. (a) Specific capacitance of the NC-5 electrode at different current densities. (b) Cyclic stability of the NC-5 electrode at current density of 2.5 A g^{-1}.

On the basis of above results, NC-5 electrode material was chosen for the detailed electrochemical measurements. The charge/discharge behavior of the NC-5 electrode at different current densities was examined in 2 M KOH electrolyte solution between 0 and 0.7 V, and the corresponding results are shown in **Figure. 3.1.7(b)**. The nonlinear charge/discharge curves further confirmed the pseudocapacitance behavior of the $NiCo_2O_4$ electrode. While increasing the discharge current density, the discharge time reduces. The specific capacitance of the electrodes can also be calculated from the GCD curves using the following equation [61].

$$C = \frac{I \times \Delta t}{m \times \Delta V} \quad \text{---------- (4)}$$

Where m is the electroactive material (g), ΔV is the potential window (V), At is the discharge time (s), and I is the constant discharge current (A). The measured specific capacitances are 62, 95, 103, 111, and 132 F g^{-1} for NC-1, NC-2, NC-3, NC-4 and NC-5 at the constant current density of 0.375 A g^{-1}, respectively. Further, the specific capacitance vs current density of the NC-5 electrode is plotted in **Figure. 3.1.8 (a)**. The decrease in specific capacitance with the increase of discharge current density was observed. The decrease of specific capacitances at higher scan rates is due to the insufficient time available for the Faradic reaction (diffusion limited behavior) of the electroactive materials. Noticeably, about ~61% of the initial specific capacitance can be retained, when the current density was increased to 5 A g^{-1}, indicates the improved capacitive behavior and high-rate capability of the $NiCo_2O_4$ electrodes. The enhanced specific capacitance of $NiCo_2O_4$ may be due to the higher surface area, short diffusion

path lengths and finally the substantial contribution of Ni^{2+}ions in the redox process.

The cyclic stability of the NC-5 electrode is also evaluated by the repeating galvanostatic charge/discharge test at a constant current density of 2.5 A g^{-1} for 2000 cycles in a potential window range of 0 to 0.7 V as shown in **Figure. 3.1.8(b)**. Interestingly, the specific capacitance increases gradually for the first 350 cycles, which may be attributed to the complete activation process of the electrode materials [58, 64]. The decrease of specific capacitance after 1500 cycles can be attributed due to the loss of adhesion of some of the electro-active material with the current collector during the repeated long term charge-discharging process [65, 66]. The NC-5 electrode retained 86% of the initial capacitance value, even after 2000 cycles, which indicates the better cyclic stability of the as-prepared $NiCo_2O_4$nanoplates electrode. Hence, $NiCo_2O_4$nanoplates electrode is considered to be one of the promising electrode materials for supercapacitor applications due to the facile and cost-effective synthesis method and improved electrochemical properties.

3.3. Conclusion

In summary, we have successfully synthesized $NiCo_2O_4$ nanoplates using a facile hydrothermal method followed by a thermal annealing process. The electrochemical charge storage behavior of the as-prepared $NiCo_2O_4$nanoplates electrode materials were investigated for supercapacitor applications. It is found that the $NiCo_2O_4$nanoplates electrode revealed a maximum specific capacitance of 332 F g^{-1} at a scan rate of 5 mV s^{-1}. Furthermore, $NiCo_2O_4$nanoplates electrode exhibited better cycle

life with capacitance retention of 86% of the initial capacitance value, even after 2000 cycles. These electrochemical studies suggested that the $NiCo_2O_4$ nanoplates area promising electrode material for supercapacitors.

4. Synthesis of Hierarchical Porous Flower-like $NiCo_2O_4$Nanosheetson Ni foam as a Binder-less Electrode for Supercapacitor Application

Highlights

- In this work, we demonstrate a large-scale growth of porous hierarchical flower-shaped nickel cobaltite (PFNC) nanosheets on Ni foam with robust adhesion as a high performance electrode material for supercapacitors via a simple hydrothermal method and post annealing treatment.
- The physico-chemical properties of the prepared binder-less electrode is studied using X-ray diffraction (XRD), Raman spectroscopy and field emission scanning electron microscopy (FE-SEM).
- The presence of porous architecture increases the electroactive cites and facilitates the fast electron and ion conduction during electrochemical measurements.
- The prepared material shows a maximum specific capacitance of 2061 Fg^{-1} (areal capacitance of 4.16 F cm^{-2}) at the current density of 5 mA cm^{-2} and 2100 F g^{-1} (4.24 F cm^{-2}) at the scan rate of 5 mV s^{-1} from charge discharge analysis and cyclic voltammetry analysis respectively.
- Overall results suggest that the prepared binder-less PFNC electrode will be a promising candidate as a positive electrode for supercapacitor applications.

4.1.Experimental Section

4.1.1. Preparation of Porous flower-shaped $NiCo_2O_4$ (PFNC)nanosheets

The growth of $NiCo_2O_4$ nanostructures on the nickel foam was achieved via a one-pot hydrothermal method and followed by post annealing treatment. Briefly, precursor solution containing $NiCl_2{\cdot}6H_2O$ and $CoCl_2{\cdot}6H_2O$ (molar ratio, 1:2) was prepared by dissolving in water and ethanol. A specified amount urea has been added gradually with the precursor solution. A slice of Ni foam was cleaned using dilute HCl, acetone, and water to remove impurities and oxide layers on the surface. The precursor solution was transferred into a 100-mL Teflon-lined autoclave (with stainless steel covering) and pre-cleaned Ni foam was immersed into the solution and kept at a constant temperature of 180℃ for 8 h. After the hydrothermal reaction, the autoclave was cooled down to room temperature and we could observe that the formation of $NiCo_2O_4$ by change of color of Ni foam into pink, indicating the uniform growth of $NiCo_2O_4$ on the nickel foam. The product obtained was washed thoroughly in distilled water and ethanol to remove residual ions and was allowed to dry in a hot-air oven overnight at 80℃. Finally, the prepared sample was calcined at 450℃ for 3 h.

4.2. Results and discussion

In this study, a facile hydrothermal technique has been used to prepare the hierarchical porous flower-like $NiCo_2O_4$ nanosheets nickel chloride and cobalt chloride precursors and its schematic illustration has been presented in **Figure.4.1.1**.

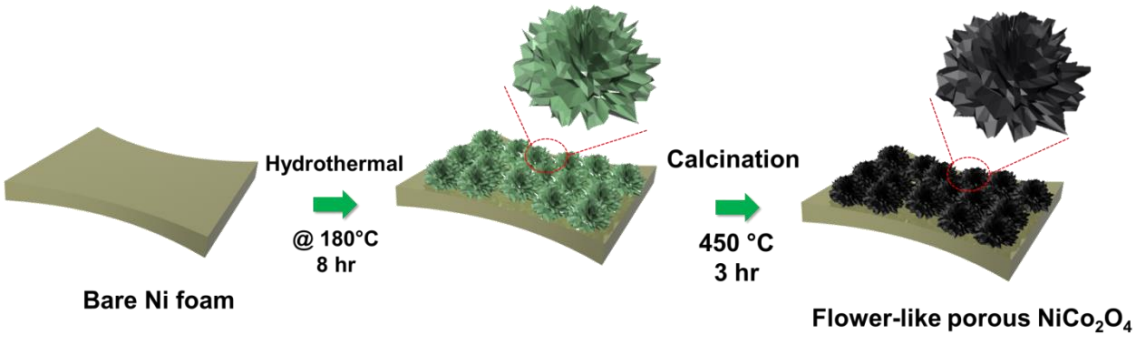

Figure.4.1.1 Schematic annotation of the preparation of porous flower-like nickel cobaltite by hydrothermal method and followed by post annealing process

The morphology of the prepared material has been presented in **Figure. 4.1.2**. As seen in **Figure. 4.1.2 (a-c)**, the samples are grown over the nickel foam substrate are uniformly distributed over the surface. As we could be observed from the high magnification images, the flower shaped morphology of $NiCo_2O_4$ over the superficial part of Ni foam has been observed. If we observe that more magnified part of the FE-SEM images as seen in **Figure. 4.1.2 (d-e)**, the typical flower-shaped hierarchical nanostructures are formed by the many petals like structure with highly porous nature. Initially, the formation of nanosheet arrays on the surface of the nickel foam obtained which has been observed from the gaps between the flowers like structure. Although, it is more notable that in some less dense part, where some petals like structure gradually grown on the nanosheet like arrays and self-assembled into a single flower like nanoarchitectured structure. The inset of **Figure 4.1.2 (a, c and e)** shows that the surface

morphology of the pristine Ni foam which suggest that the smooth surface of Ni foam. After grown of sample, more significantly, the high small porous nature on the surface

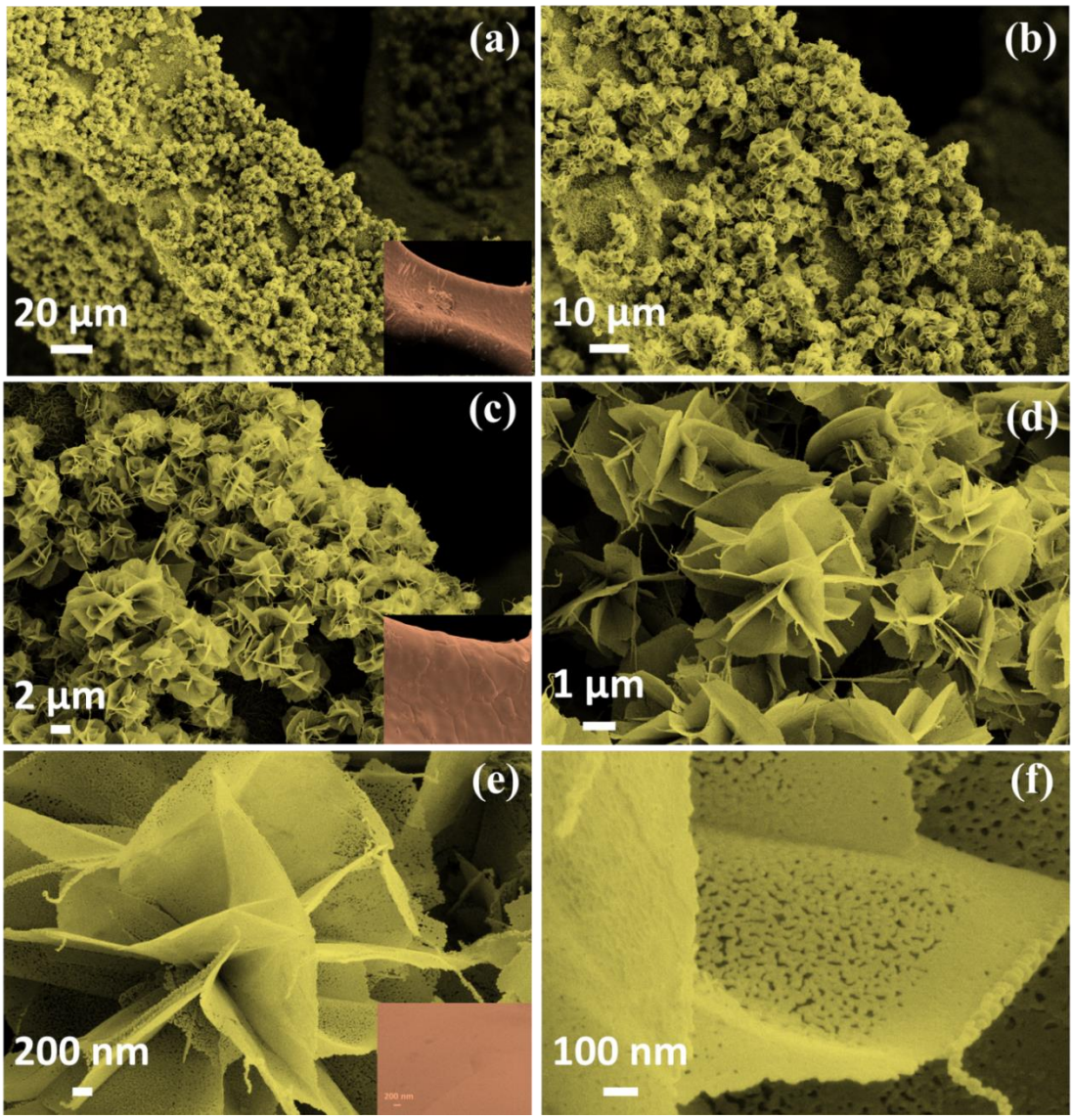

Figure.4.1.2. FE-SEM images of the prepared nickel cobaltite sample at different magnifications, 20 µm (a), 10 µm (b), 2 µm (c), 1 µm (d), 200 nm (e) and 100 nm (f)

of the petals of flowers is created by the evolution of gas (the use of high content of urea leads to release of CO_2 and ammonia gas) during crystal transformation from the surface at the temperature of 450 ℃ in air atmosphere. This porous structure will provide to improved specific surface area which leads to the high ion penetration during electrochemical reaction. The phase purity and crystal structure of the prepared hierarchical flower-shaped $NiCo_2O_4$ nanosheets is investigated using XRD pattern technique and presented in **Figure.4.1.3**. The bare Ni foams shows three major peaks at the diffraction angle of 44.6°, 51.9°, and 76.7° are corresponding to the Ni foam diffraction planes. After hydrothermal reaction, the additional peaks are observed which can be clearly indexed that the formation of cubic $NiCo_2O_4$ with a spinel structure [67, 68]. The diffraction angles at 19, 31.2, 36.8, 43.4, 59.1, 65° are attributed to the (111), (220), (311), (400), (511) and (440) diffraction planes respectively. These peaks are well consistent with the Joint Committee Pattern for Diffraction Standards (PDF No 73-1702). There is no any other peaks are observed suggesting that the prepared hierarchical $NiCo_2O_4$ nanoflowers are formed with high purity without any impurities.

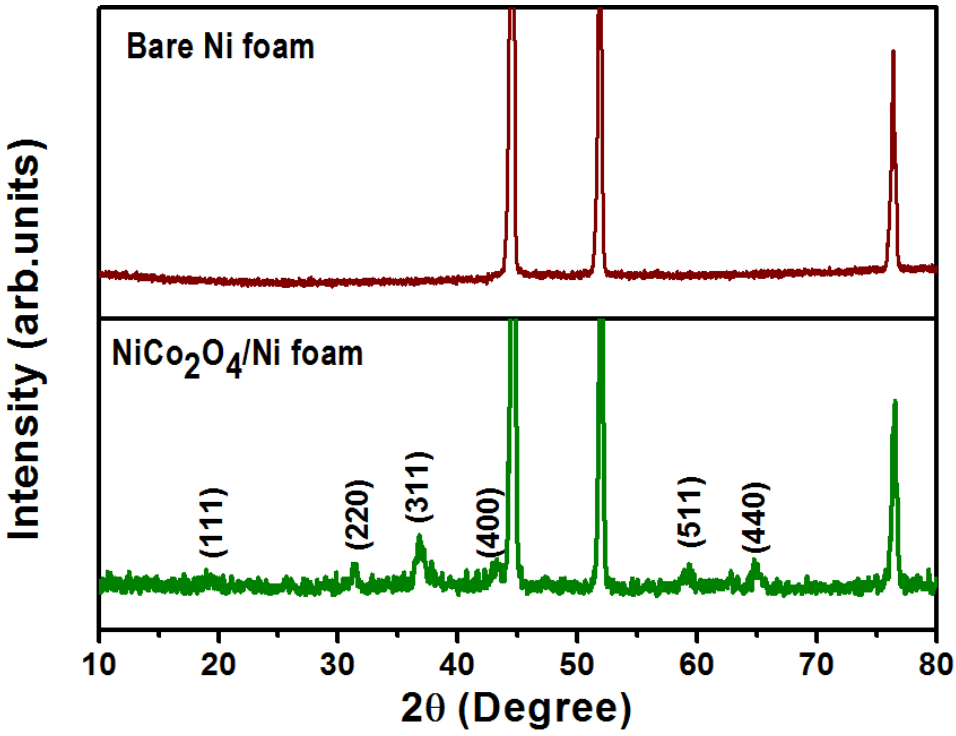

Figure.4.1.3. XRD pattern of the prepared nickel cobaltite grown on Ni foam and bare Ni foam

Initially, during decomposition of hydrolysis of urea with the metal ions, the formation of OH^- and CO_3^{2-} ions are obtained which results in the generation of metal carbonate hydroxyl species. Later, this carbonate hydroxyl species are converted into the pure $NiCo_2O_4$ after post annealing process. Then this obtained product is well indexed with the cubic spinel structure. In order to further evaluate the chemical composition of the prepared materials, we have measured X-ray photoelectron spectroscopy technique on the surface of the sample and corresponding results were presented in **Figure.4.1.4**. The survey spectrum of the sample (**Figure 4.1.4 (a)**) indicates that the presence of the

elements on the surface such as Ni, Co, O as well as carbon from the reference and absence of any other foreign particles/impurities.

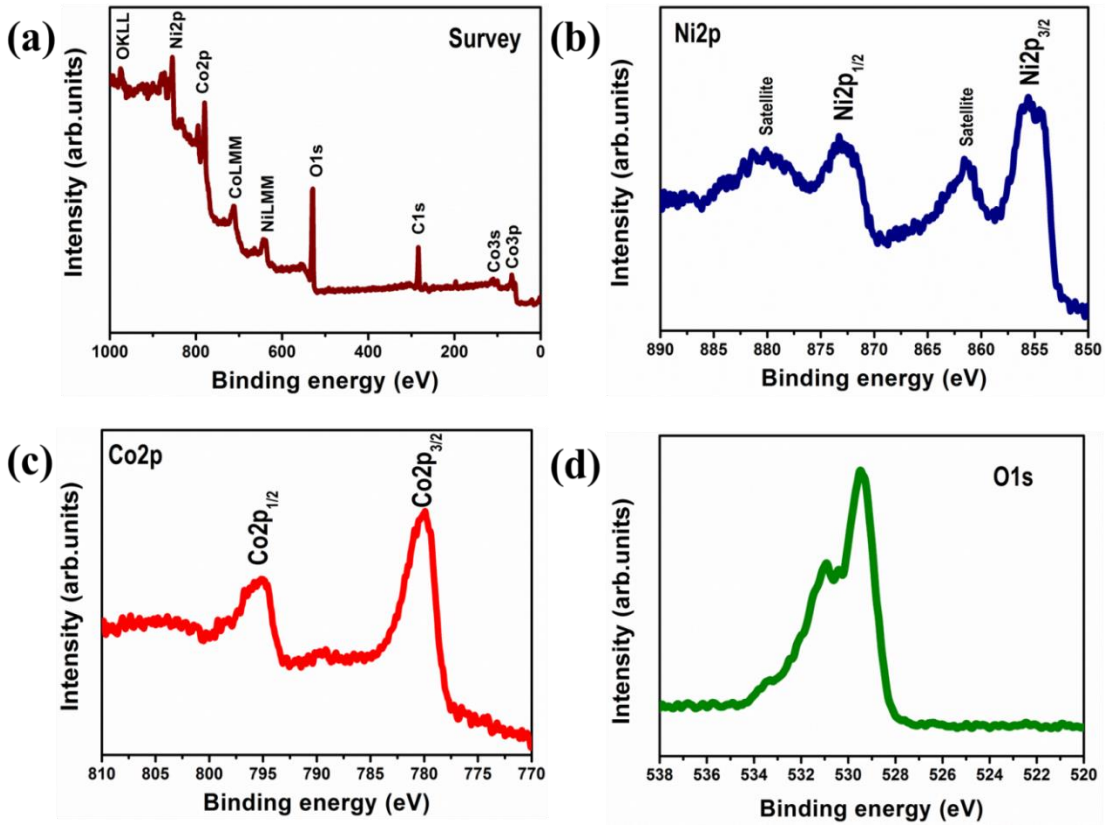

Figure.4.1.4. X-ray photoelectron spectroscopy for the prepared sample: Survey spectrum (a), Ni2p core-level spectrum (b), Co2p core-level (c) and O1s core-level spectrum (d) of the prepared $NiCo_2O_4$/Ni foam sample

As can be seen form **Figure 4.1.4b**, the characteristic peak of Ni^{2+} and Ni^{3+} are observed with two shake-up satellite peaks. The peak at ~855 eV and ~873 eV are corresponding to the $Ni2p_{3/2}$ and $Ni2p_{1/2}$ respectively which are clearly indicated that the presence of Ni2p core-level spectra [69]. In Co2p core-level spectra (shown in **Figure 4.1.4 (c)**), two types of cobalt species can also be found and ascribed to the species

containing Co(II) and Co(III) ions over the surface. More importantly, the peaks at the binding energies of ~780 eV and ~795 eV are corresponding to the presence of $Co2p_{3/2}$ and $Co2p_{1/2}$ respectively [70]. The high resolution O1s core-level spectrum is presented in **Figure 4.1.4d**. There are three peaks could be easily identified in the spectrum. The binding energy at 529.4 eV is typical oxygen-metal bond. The peak at 531 eV is generally associated with the contaminants, defects and a number of other chemical species such as hydroxyls, lattice oxygen, chemisorbed oxygen, or the species intrinsic to the surface the spinel structure [70, 71]. Further, the small band at ~533 eV could be assigned to the multiplicity of physisorbed/chemisorbed water molecules over or near the surface. The O^{2-} species in $NiCo_2O_4$ could be ascribed to the O1s spectrum at the binding energies of 529.4 eV and 531 eV [70, 72]. These results from the XPS measurement demonstrate that the electron couples of Ni^{3+}/Ni^{2+} and Co^{3+}/Co^{2+} species are coexisting in the prepared hierarchical porous flower-like $NiCo_2O_4$ sample.

An electrochemical performance of the prepared PFNC electrode material is investigated in detail. **Figure.4.1.5 (a, b)** shows the CV curves at the different scan rates in a potential range of -0.1 to 0.6 V. The CV curves suggest that the prepared material shows a pair of redox peaks which might be originates from the faradaic reaction related to the M-O or M-O-OH (where M stands for either Ni or Co) [73]

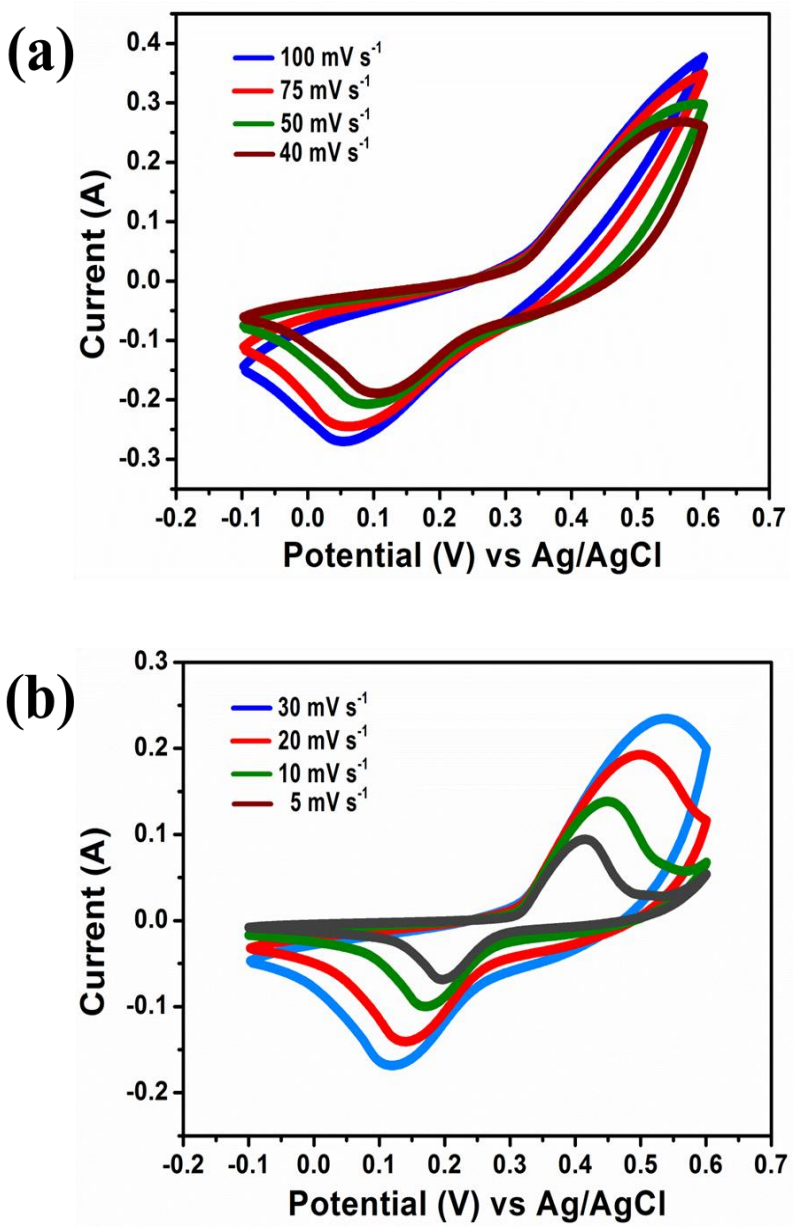

Figure.4.1.5. Cyclic voltammetry curves at the different scan rates, from 100 mV s^{-1} to 40 mV s^{-1} (a), from 30 mV s^{-1} to 5 mV s^{-1} (b),

More importantly, although two redox couples of Co^{2+}/Co^{3+} and Ni^{2+}/Ni^{3+} are available in the prepared nanostructures, there is no two distinct peaks of that Co^{2+}/Co^{3+} and Ni^{2+}/Ni^{3+} are not observed in CV curves since the Co_3O_4 and NiO have similar redox potential. The shape of CV curves is almost similar and the current is linearly increases with respect to the scan rates suggesting the good kinetic reversibility of the prepared PFNC on Ni foam electrode. Notably, on 100 mV of the peak potential shift occurred even 10 times increase in scan rates which is because of low polarization of the prepared PFNC electrode material.

Similarly, the GCD measurements measured at different current densities from 100 mA cm^{-2} to 30 mA cm^{-2} (**Figure. 4.1.6a**) and from 25 mA cm^{-2} to 5 mA cm^{-2}) presented in **Figure. 4.1.6(b**) are also confirm that the presence of a pair of redox couple which originates from the faradaic reaction. This redox reaction in the alkaline electrolyte is explained as follows [74];

$$NiCo_2O_4 + OH^- + H_2O \leftrightarrow NiOOH + 2CoOOH + e^- \quad \text{---------- (3)}$$

$$CoOOH + OH^- \leftrightarrow CoO_2 + H_2O + e^- \quad \text{---------- (4)}$$

All the numerical specific capacitances are calculated using the cyclic voltammetry analysis and discharge curves of the charge discharge curves and presented in **Figure. 4.1.7 a, b**.

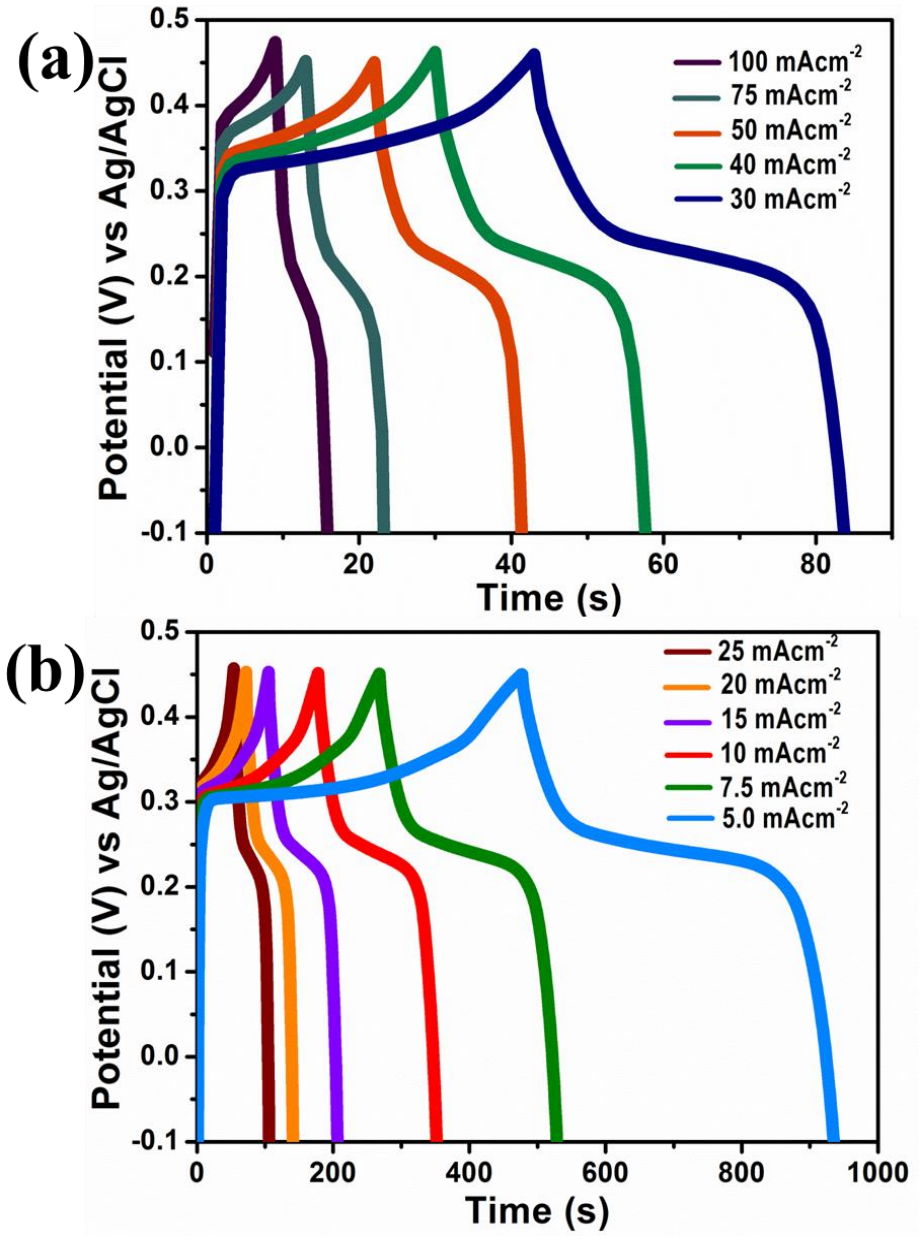

Figure. 4.1.6. Galvanostatic charge discharge analysis at different current densities, from 100 mA cm^{-2} to 30 mA cm^{-2} (c) and 25 mA $cm^{-2}$to 5 mA cm^{-2}

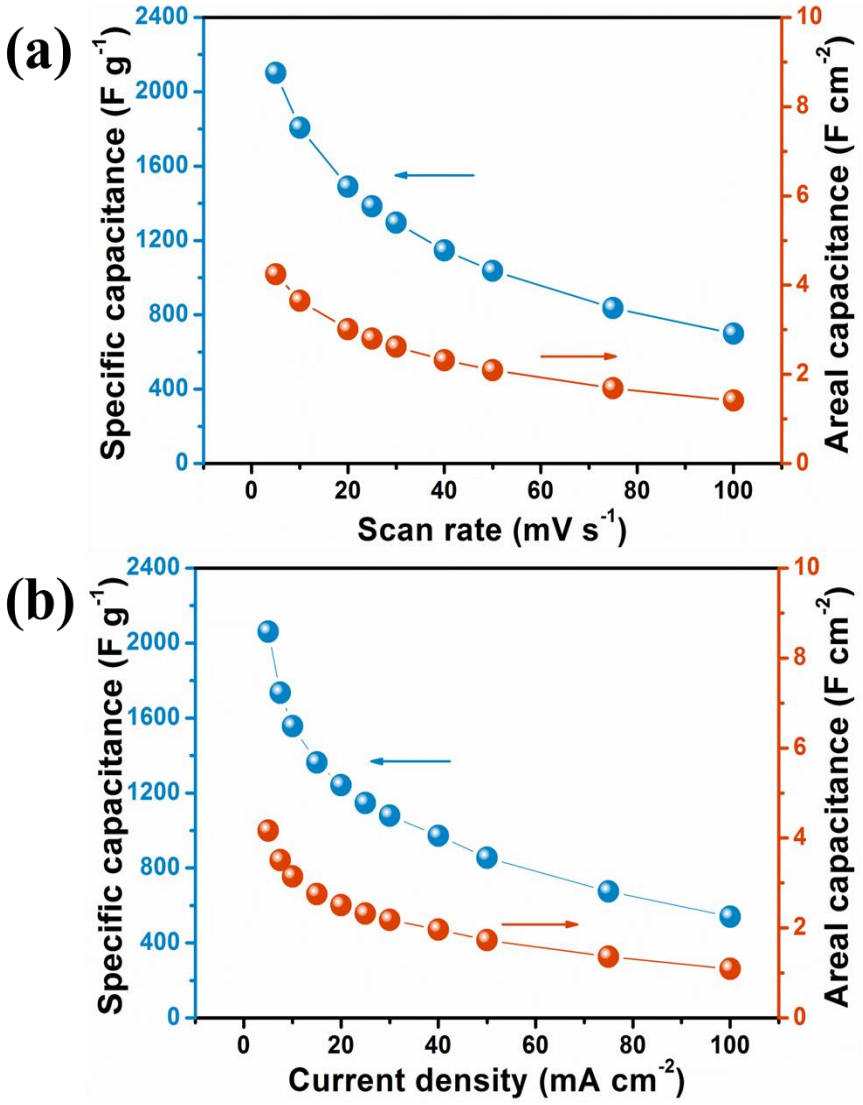

Figure.4.1.7. Gravimetric and areal capacitances with respect to the scan rates (a) and current densities (b)

The maximum obtained gravimetric and areal capacitances from CV curves are 2061 F g^{-1} and 4.16 F cm^{-2} respectively (**Figure. 4.1.7 (a)**). Also, the maximum calculated gravimetric and areal capacitances from CV curves are 2100 F g^{-1} and 4.24 F cm^{-2} respectively (**Figure. 4.1.7 (b)**).The calculated specific capacitances from both

techniques are almost same. As can be seen from the GCD curves, when increasing the current density, the obtained specific capacitance tends to decrease.

As shown in **Figure. 4.1.7 (b)**, even when increasing the current density from 5 mA cm^{-2} to 20 mA cm^{-2}, there is very low capacitance loss is observed which suggesting the excellent rate capability behavior at the lower current densities. In addition, it is noteworthy that the substantial improvement in capacitive performance at the high current density is associated to efficient utilization of an electroactive surface of the superior porous flower-shaped PFNC superstructure electrodes. The prepared flower shaped superstructure consisting of the porous nano-petals could considerable providing the electroactive sites for faradaic reaction. In this case, the porous flower shaped nano architectures facilitates a quicker electrolyte ion penetration process into each porous petal shaped matrix by decreasing the diffusion distances of hydroxyl ions to the active electrode materials for faradaic reaction. Therefore, even at higher current density, the high specific capacitance is obtained which is due to even high current density, the large portion of active sites are available for the faradaic reaction. The achieved gravimetric/areal capacitance is higher than the previous reports such as 3D hierarchical flower-shaped nickel cobaltite ($NiCo_2O_4$) microspheres prepared by microwave method (1006 F g^{-1}) [75], urchin-like $NiCo_2O_4$ by hydrothermal method (1650 F g^{-1}) [76], mesoporous $NiCo_2O_4$ nanoflowers by reflux method (1635 F g^{-1}) [77], Nano $NiCo_2O_4$ coral-like architecture microwave assisted method (870 Fg^{-1}) [78], Porous $NiCo_2O_4$ nanowires by micro emulsion method (1197 F g^{-1}) [79], 3D porous $NiCo_2O_4$/Ni by

electrochemical deposition method (1.139 F cm^{-2}) [80], flower like $NiCo_2O_4$ nanosheets by solvothermal technique (1440 Fg^{-1}) [81]. The cyclic stability of the electrode materials is one of the important method is to find out the electrode's durability. We have performed cyclic stability of the prepare PFNC electrode using galvanostatic charge discharge analysis at the current density of 50 mA cm^{-2} for continuous 2000 cycles and shown in **Figure.4.1.8**. As the porous electrode material have three states during stability such as initial activation period, steady state and degradation periods, the initial 50 cycles, the specific capacitance slight increased and started to decrease [75, 82]. Within 500 cycles, the capacitance was lost upto 94.5%; however, even upto 1500 cycles, the capacitance is retained upto 92.5%. At the end of 2000 cycles, about 88.5% of its initial capacitance is retained suggesting the better cyclic stability of the prepared PFNC electrodes.

Electrochemical impedance spectroscopy is one of the important techniques in order to evaluate the capacitive nature of electrode materials. The **inset of Figure.4.1.8** shows the Nyquist plot before and after cyclic stability tests. Both the plot shows two common features such as semi-circle region at the high frequency and straight line at the lower frequency region. After 2000 cycles, the solution and charge transfer resistance is slightly increased which suggesting the conductivity of the electrode material is decreased slightly. Thus, the prepared materials show its good durability behavior even after long cycles. Overall, results suggested the prepared PFNC electrode materials will be the suitable candidate as a positive electrode materials for supercapacitor applications.

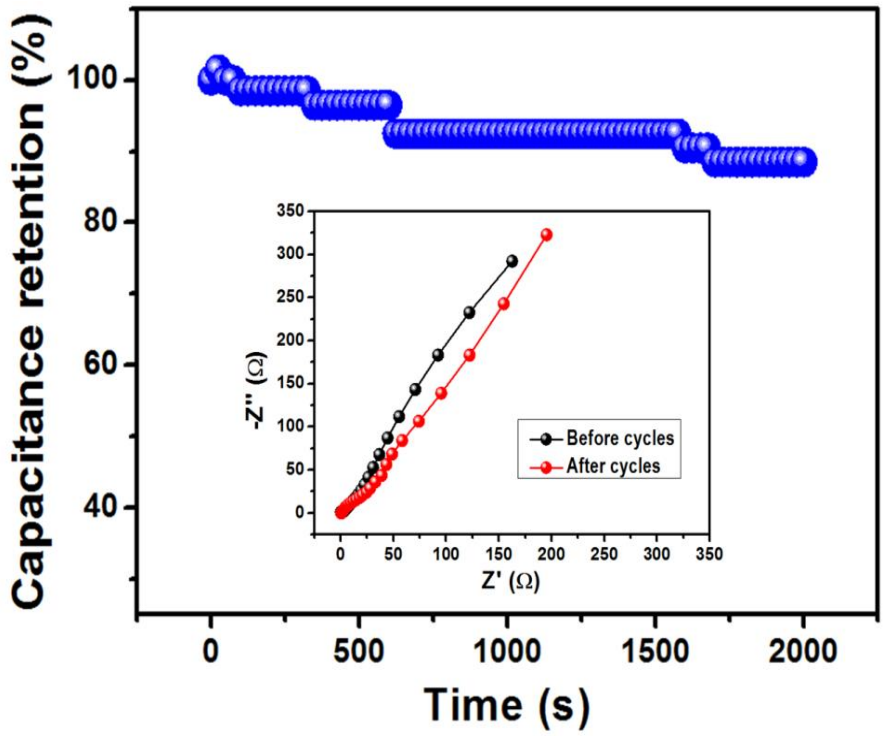

Figure.4.1.8. Cyclic stability test measured using galvanostatic charge discharge analysis for 2000 cycles, inset shows the Nyquist plot before and after cyclic stability

4.3.Conclusion

We have successfully prepared highly porous binder-free $NiCo_2O_4$ nanosheets on Ni foam substrate using a facile hydrothermal method followed by post annealing process. The prepared electrode material was well characterized using various techniques. From the morphological analysis, the highly porous nature $NiCo_2O_4$ nanopetals are observed which facilitates the improved surface area for the electrolyte penetration. The electrochemical charge storage behavior of the prepared $NiCo_2O_4$

nanosheets was investigated as a positive electrode for supercapacitor applications. It is noteworthy that the prepared porous binder-free $NiCo_2O_4$ on Ni foam electrode exhibited a maximum gravimetric capacitance of 2100 F g^{-1} by GCD measurement at the current density of 5 mA cm^{-2} which is almost equal to the capacitance (2061 Fg^{-1}) calculated by CV analysis at the scan rate of 5 mV s^{-1}. Moreover, porous binder-free $NiCo_2O_4$ nanopetals electrode exhibited better durability with capacitance retention of 88.5% of the initial value, even after continuous 2000 cycles. Overall, the obtained electrochemical results suggested that the binder-free $NiCo_2O_4$ nanosheets are a promising candidate as a positive electrode material for supercapacitor applications.

5. References

1. A.S. Arico, P. Bruce, B. Scrosati, J.-M. Tarascon, W. van Schalkwijk, Nanostructured materials for advanced energy conversion and storage devices, Nat Mater, 4 (2005) 366-377.
2. P. Simon, Y. Gogotsi, Materials for electrochemical capacitors, Nat Mater, 7 (2008) 845-854.
3. G. Wang, L. Zhang, J. Zhang, A review of electrode materials for electrochemical supercapacitors, Chem Soc Rev, 41 (2012) 797-828.
4. C.A. Vincent, B. Scrosati, "Modern batteries: An introduction to electrochemical power sources", Arnold, London (1997).
5. S.U. Falk, S. J. Salkind, "Alkaline storage batteries", Wiley, New York (1969)
6. S.W. Lee, B.M. Gallant, H R. Byon, P.T. Hammond, Y. Shao-Horn, Nanostructured carbon- based electrodes: bridging the gap between thin-film lithium-ion batteries and electrochemical capacitors, Energy. Environ Sci., 4 (2011) 1972-1985.
7. F. Zhang, T. Zhang, X. Yang, L. Zhang, K. Leng, Y. Huang, Y. Chen, A high-performance supercapacitor-battery hybrid energy storage device based on graphene-enhanced electrode materials with ultrahigh energy density, Energy. Environ Sci., 6 (2013) 1623-1632.
8. L.L. Zhang, R. Zhou, X.S. Zhao, Graphene-based materials as supercapacitor electrodes, J. Mater. Chem., 20 (2010) 5983-5992.

9. W. Li, G. Li, J. Sun, R. Zou, K. Xu, Y. Sun, Z. Chen, J. Yang, J. Hu, Hierarchical heterostructures of MnO2 nanosheets or nanorods grown on Au-coated Co_3O_4 porous nanowalls for high-performance pseudocapacitance, Nanoscale, 5 (2013) 2901-2908.
10. C. Liu, F. Li, L.-P. Ma, H.-M. Cheng, Advanced Materials for Energy Storage, Adv. Mater., 22 (2010) E28-E62.
11. W. Li, K. Xu, L. An, F. Jiang, X. Zhou, J. Yang, Z. Chen, R. Zou, J. Hu, Effect of temperature on the performance of ultrafine MnO2 nanobelt supercapacitors, J. Mater. ChemA., 2 (2014) 1443-1447.
12. M. Zhi, C. Xiang, J. Li, M. Li, N. Wu, Nanostructured carbon-metal oxide composite electrodes for supercapacitors: a review, Nanoscale, 5 (2013) 72-88.
13. F. Y. Cheng, H. B. Wang, Z. Q. Zhu, Y. Wang, T. R. Zhang, Z. L. Tao, J. Chen, Porous $LiMn_2O_4$ nanorods with durable high-rate capability for rechargeable Li-ion batteries, Energy. Environ. Sci., 4 (2011) 3668–3675.
14. L. L. Li, S. J. Peng, Y. L. Cheah, J. Wang, P. F. Teh, Y. W. Ko,C. L. Wong and M. Srinivasan, Electrospun eggroll-like $CaSnO_3$ nanotubes with high lithium storage performance Nanoscale, 5 (2013) 134–138.
15. F. M. Courtel, H. Duncan, Y. Abu-Lebdeh and I. J. Davidson, High capacity anode materials for Li-ion batteries based on spinel metal oxides AMn_2O_4 (A = Co, Ni, and Zn) J. Mater. Chem., 21 (2011) 10206–10218.
16. G. Wang, L. Zhang, J. Zhang, A review of electrode materials for electrochemical

supercapacitors, Chem. Soc. Rev., 41 (2012) 797-828.

17. S. Makino, Y. Yamauchi, W. Sugimoto, Synthesis of electro-deposited ordered mesoporous RuOx using lyotropic liquid crystal and application toward micro-supercapacitors. J. Power Sources 227 (2013) 153–160.
18. M. Toupin, T. Brousse, D. Belanger, Charge storage mechanism of MnO_2 electrode used in aqueous electrochemical capacitor. Chem. Mater. 16 (2004) 3184–3190.
19. J. Ji, L.L. Zhang, H. Ji, Y. Li, X. Zhao, X. Bai, X. Fan, F. Zhang, R.S. Ruoff, Nanoporous $Ni(OH)_2$ thin film on 3D ultrathin-graphite foam for asymmetric supercapacitor. ACS Nano 7 (2013) 6237–6243.
20. J. Liu, J. Jiang, C. Cheng, H. Li, J. Zhang, H. Gong, H. J. Fan, Co_3O_4 nanowire@MnO_2 ultrathin nanosheet core/shell arrays: a new class of high-performance pseudocapacitive materials. Adv. Mater. 23, (2011) 2076–2081.
21. E -H. Liu, W. Li, J. Li, X -Y. Meng, R. Ding, S -T. Tan, Preparation and characterization of nanostructured NiO/MnO2 composite electrode for electrochemical supercapacitors, Mater. Res. Bull., 44 (2009) 1122-1126.
22. J.-K. Chang, W.-C. Hsieh, W.-T. Tsai, Effects of the Co content in the material characteristics and supercapacitive performance of binary Mn-Co oxide electrodes, J. Alloys Compd, 461 (2008) 667-674.
23. F. Yunyun, L. Xu, Z. Wankun, Z. Yuxuan, Y. Yunhan, Q. Honglin, X. Xuetang, W. Fan, Spinel CoMn2O4 nanosheet arrays grown on nickel foam for high-performance supercapacitor electrode, Appl. Surf. Sci., 357, Part B (2015) 2013-2021.

24. R. Wang, X. Yan, Superior asymmetric supercapacitor based on Ni-Co oxide nanosheets and carbon nanorods, Sci. Rep., 4 (2014).
25. M.-T. Lee, J.-K. Chang, Y.-T. Hsieh, W.-T. Tsai, Annealed Mn-Fe binary oxides for supercapacitor applications, J. Power Sources, 185 (2008) 1550-1556.
26. Y. Xie, C. Huang, L. Zhou, Y. Liu, H. Huang, Supercapacitor application of nickel oxide- titania nanocomposites, Compos. Sci. Technol., 69 (2009) 2108-2114.
27. M. Jayalakshmi, N. Venugopal, K.P. Raja, M.M. Rao, Nano SnO_2-Al_2O_3 mixed oxide and SnO_2-Al_2O_3-carbon composite oxides as new and novel electrodes for supercapacitor applications, J. Power Sources, 158 (2006) 1538-1543.
28. J.-M. Luo, B. Gao, X.-G. Zhang, High capacitive performance of nanostructured Mn-Ni-Co oxide composites for supercapacitor, Mater. Res. Bull., 43 (2008) 1119-1125.
29. T.-C. Wen, H.-M. Kang, Co-Ni-Cu ternary spinel oxide-coated electrodes for oxygen evolution in alkaline solution, Electrochim. Acta, 43 (1998) 1729-1745.
30. D.-L. Fang, Z.-D. Chen, B.-C. Wu, Y. Yan, C.-H. Zheng, Preparation and electrochemical properties of ultra-fine Mn-Ni-Cu oxides for supercapacitors, Mater. Chem. Physics, 128 (2011) 311-316.
31. C. Yuan, H.B. Wu, Y. Xie, X.W. Lou, Mixed Transition-Metal Oxides: Design, Synthesis, and Energy-Related Applications, Angew. Chem. Int. Ed., 53 (2014) 1488-1504.
32. C. Yan, H. Jiang, T. Zhao, C. Li, J. Ma, P S. Lee, Binder-free $Co(OH)_2$nanoflake-

ITO nanowire heterostructured electrodes for electrochemical energy storage with improved high-rate capabilities, J. Mater. Chem, 21 (2011) 10482-10488.

33. G. Hongyi, W. Ge, Y. Mu, T. Li, Y. Jie, Novel tunable hierarchical Ni-Co hydroxide and oxide assembled from two-wheeled units, Nanotechnology, 23 (2012) 015607.
34. J.Y. Dong, X.T. Zhang, The preparation and electrochemical characterization of urchin-like $NiCo_2O_4$ nanostructures, Appl. Surf. Sci., 332 (2015) 247-252.
35. B. Sarma, R.S. Ray, S.K. Mohanty, M. Misra, Synergistic enhancement in the capacitance of nickel and cobalt based mixed oxide supercapacitor prepared by electrodeposition, Appl. Surf. Sci., 300 (2014) 29-36.
36. M. Yu, J. Chen, Y. Ma, J. Zhang, J. Liu, S. Li, J. An, Hydrothermal synthesis of $NiCo_2O_4$ nanowires/nitrogen-doped graphene for high-performance supercapacitor, Appl.Surf.Sci. 314 (2014) 1000-1006.
37. . Zhang, H. Gao, Q. Yang, X.T. Zhang, M.Y. Zhang, L.L. Xu, Effect of temperature on pseudocapacitance performance of carbon fiber@$NiCo_2O_4$@$Ni(OH)_2$ core-shell nanowire array composite electrodes, Appl. Surf. Sci., 356 (2015) 167-172.
38. A. Trunov, Analysis of oxygen reduction reaction pathways on Co3O4, NiCo2O4, Co_3O_4- Li_2O, NiO, NiO-Li_2O, Pt, and Au electrodes in alkaline medium, Electrochim. Acta, 105 (2013) 506-513.
39. Y. Zhu, Z. Wu, M. Jing, W. Song, H. Hou, X. Yang, Q. Chen, X. Ji, 3D network-like mesoporous $NiCo_2O_4$ nanostructures as advanced electrode material for supercapacitors, Electrochim. Acta, 149 (2014) 144-151.

40. G. Zhang, X.W. Lou, General Solution Growth of Mesoporous $NiCo_2O_4$ Nanosheets on Various Conductive Substrates as High-Performance Electrodes for Supercapacitors, Adv. Mater., 25 (2013) 976-979.
41. H. Jiang, J. Ma, C. Li, Hierarchical porous $NiCo_2O_4$ nanowires for high-rate supercapacitors, Chem Comm., 48 (2012) 4465-4467.
42. L. Li, Y. Cheah, Y. Ko, P. Teh, G. Wee, C. Wong, S. Peng, M. Srinivasan, The facile synthesis of hierarchical porous flower-like $NiCo_2O_4$ with superior lithium storage properties, J. Mater. Chem. A, 1 (2013) 10935-10941.
43. Q. Wang, B. Liu, X. Wang, S. Ran, L. Wang, D. Chen, G. Shen, Morphology evolution of urchin-like $NiCo_2O_4$ nanostructures and their applications as psuedocapacitors and photo electrochemical cells, J. Mater Chem., 22 (2012) 21647-21653.
44. J. Pu, J. Wang, X. Jin, F. Cui, E. Sheng, Z. Wang, Porous hexagonal $NiCo_2O_4$ nanoplates as electrode materials for supercapacitors, Electrochim. Acta, 106 (2013) 226-234.
45. S. Chen, W. Xing, J. Duan, X. Hu, S.Z. Qiao, Nanostructured morphology control for efficient supercapacitor electrodes, J. Mater. Chem. A, 1 (2013) 2941-2954.
46. T. Zhu, J.S. Chen, X.W. Lou, Shape-controlled synthesis of porous Co3O4 nanostructures for application in supercapacitors, J. Mater. Chem., 20 (2010) 7015-7020.
47. S.K. Meher, G.R. Rao, Ultralayered Co_3O_4 for High-Performance Supercapacitor

Applications, J. Phys. Chem. C, 115 (2011) 15646-15654.

48. J. S. Hu, L. S. Zhong, W. G. Song, L. Wan, Synthesis of hierarchically structured metal oxides and their application in heavy metal ion removal, J. Adv. Mater. 20 (2008) 2977−2982.
49. W. M. Liu, T. T. Gao, Y. Yang, Q. Sun, Z. W. Fu, A hierarchical three-dimensional $NiCo_2O_4$ nanowire array/carbon cloth as an air electrode for nonaqueous Li–air batteries, Phys. Chem. Chem. Phys. 15 (2013) 15806−15810.
50. K. Byrappa and M. Yoshimura: Handbook of Hydrothermal Technology (Noyes Publications/William Andrew Publishing LLC, U.S.A. 2001).
51. S. Sōmiya, and R. Roy, Hydrothermal synthesis of fine oxide powders, Bull.Mater. Sci. 23(6) (2000) 453–460.
52. Y. Zhu, X. Ji, Z. Wu, W. Song, H. Hou, Z. Wu, X. He, Q. Chen, C.E. Banks, Spinel NiCo2O4 for use as a high-performance supercapacitor electrode material: Understanding of its electrochemical properties, J. Power Sources, 267 (2014) 888-900.
53. Y. Zhu, X. Pu, W. Song, Z. Wu, Z. Zhou, X. He, F. Lu, M. Jing, B. Tang, X. Ji, High capacity NiCo2O4 nanorods as electrode materials for supercapacitor, J. Alloys Compd, 617 (2014) 988-993.
54. J. Xu, Y. Dong, J. Cao, B. Guo, W. Wang, Z. Chen, Microwave-incorporated hydrothermal synthesis of urchin-like Ni(OH)2-Co(OH)2 hollow microspheres and their supercapacitor applications, Electrochim. Acta, 114 (2013) 76-82.

55. H. Xiao, F. Qu, X. Wu, Ultrathin NiO nanoflakes electrode materials for supercapacitors, Appl .Surf. Sci., 360, Part A (2016) 8-13.
56. S. Zhao, T. Liu, D. Shi, Y. Zhang, W. Zeng, T. Li, B. Miao, Hydrothermal synthesis of urchin-like MnO2 nanostructures and its electrochemical character for supercapacitor, Appl .Surf. Sci., 351 (2015) 862-868.
57. V. Gupta, S. Gupta, N. Miura, Electrochemically synthesized nanocrystalline spinel thin film for high performance supercapacitor, J. Power Sources, 195 (2010) 3757-3760.
58. X.Y. Liu, Y.Q. Zhang, X.H. Xia, S.J. Shi, Y. Lu, X.L. Wang, C.D. Gu, J.P. Tu, Self-assembled porous NiCo2O4 hetero-structure array for electrochemical capacitor, J. Power Sources, 239 (2013) 157-163.
59. X. Wang, X. Han, M. Lim, N. Singh, C L. Gan, M. Jan, P S. Lee, Nickel Cobalt Oxide- Single Wall Carbon Nanotube Composite Material for Superior Cycling Stability and High- Performance Supercapacitor Application, J. Phys .Chem. C, 116 (2012) 12448-12454.
60. L.-B. Kong, J.-W. Lang, M. Liu, Y.-C. Luo, L. Kang, Facile approach to prepare loose- packed cobalt hydroxide nano-flakes materials for electrochemical capacitors, J. Power Sources, 194 (2009) 1194-1201.
61. A. Ramadoss, S.J. Kim, Improved activity of a graphene-TiO2 hybrid electrode in an electrochemical supercapacitor, Carbon, 63 (2013) 434-445.
62. J. Chen, D.H. Bradhurst, S.X. Dou, H.K. Liu, Nickel Hydroxide as an Active

Material for the Positive Electrode in Rechargeable Alkaline Batteries, J. Electrochem. Soc., 146 (1999) 3606-3612.

63. T.N. Ramesh, P.V. Kamath, C. Sivakumar, Correlation of Structural Disorder with the Reversible Discharge Capacity of Nickel Hydroxide Electrode, J. Electrochem. Soc., 152 (2005) A806-A810.
64. W. Li, J. Shao, Q. Liu, X. Liu, X. Zhou, J. Hu, Facile synthesis of porous Mn2O3 nanocubics for high-rate supercapacitors, Electrochim. Acta, 157 (2015) 108-114.
65. Rusi, S.R. Majid, Green synthesis of in situ electrodeposited rGO/MnO2 nanocomposite for high energy density supercapacitors, Sci. Rep., 5 (2015) 16195.
66. J. D. Yan, Y. Liu, Y. Li, R. Zhuo, Z. Wu, P. Ren, S. Li, J. Wang, P. Yan, Z. Geng, Synthesis and electrochemical properties of MnO2/rGO/PEDOT:PSS ternary composite electrode material for supercapacitors, Mater. Lett, 127 (2014) 53-55.
67. B. Cui, H. Lin, J. B. Li, X. Li, J. Yang, J. Tao, Core–Ring Structured $NiCo_2O_4$ Nanoplatelets: Synthesis, Characterization, and Electrocatalytic Applications, Adv. Funct.Mater, 18 (2008) 1440–1447.
68. T. Y. Wei, C. H. Chen, H. C. Chien, S. Y. Lu and C. C. Hu, Cost-Effective Supercapacitor Material of Ultrahigh Specific Capacitances: Spinel Nickel Cobaltite Aerogels from an Epoxide-Driven Sol–Gel Process,Adv. Mater., 22 (2010) 347–351.
69. J.G. Kim, D. Pugmire, D. Battaglia, M. Langell, Analysis of the $NiCo_2O_4$ spinel surface with Auger and X-ray photoelectron spectroscopy, Appl. Surf. Sci.165 (2000) 70−84.

70. J. Marco, J. Gancedo, M. Gracia, J. Gautier, E. Rıos, F. Berry, Characterization of the nickel cobaltite, $NiCo_2O_4$, prepared by several methods: an XRD, XANES, EXAFS, and XPS study,J. Solid State Chem. 153 (2000) 74−81.

71. T. Choudhury, S. Saied, J. Sullivan, A.M. Abbot, Reduction of oxides of iron, cobalt, titanium and niobium by low-energy ion bombardment, J. Phys. D: Appl.Phys. 22 (1989) 1185.

72. J. H. Zhong, A. L. Wang, G. R. Li, J. W. Wang, Y. N. Ou, Y. X. Tong, $Co_3O_4/Ni(OH)_2$ composite mesoporous nanosheet networks as a promising electrode for supercapacitor applications, J. Mater. Chem. 2012, 22, 5656−5665.

73. C. Yuan, J. Li, L. Hou, X. Zhang, L. Shen, and X. W. D. Lou, Ultrathin Mesoporous $NiCo_2O_4$ Nanosheets Supported on Ni Foam as Advanced Electrodes for Supercapacitors, Adv. Funct. Mater. 22 (2012) 4592-4597.

74. Q. Zhou, X. Wang, Y. Liu, Y. He, Y. Gao, J. Liu, High Rate Capabilities of $NiCo_2O_4$-Based Hierarchical Superstructures for Rechargeable Charge Storage, J. Electrochem.Soc, 161 (12) (2014) A1922-A1926.

75. Y. Lei, J. Li, Y. Wang, L. Gu, Y. Chang, H. Yuan, D. Xiao, Rapid Microwave-Assisted Green Synthesis of 3D Hierarchical Flower-Shaped $NiCo_2O_4$ Microsphere for High-Performance Supercapacitor, ACS Appl. Mater. Interfaces 6 (2014) 1773−1780.

76. Q. Wang, B. Liu, X. Wang, S. Ran, L. Wang, D. Chen, G. Shen, Morphology evolution of urchin-like $NiCo_2O_4$nanostructures and their applications as psuedocapacitors and photoelectrochemical cells, J. Mater. Chem. 22 (2012) 21647−21653.

77. K. Xu, J. Yang, S. Li,Q. Liu, J. Hu, Facile synthesis of hierarchical mesoporous $NiCo_2O_4$ nanoflowers with large specific surface area for high-performance supercapacitors, Mater Let. 187 (2017) 129–132.

78. Y. Tao, L. Ruiyi, L. Zaijun, F. Yinjun, A facile and scalable strategy for synthesis of size-tunable $NiCo_2O_4$ with nanocoral-like architecture for high-performance supercapacitors, Electrochim. Acta 134 (2014) 384–392.

79. C. An, Y. Wangn, Y. Huang, Y. Xu, L. Jiao, H. Yuan, Porous $NiCo_2O_4$ nanostructures for high performance supercapacitors via a micro emulsion technique, Nano Energy 10 (2014) 125–134.

80. T. Wang, Y. Guo, B. Zhao, S. Yu , H.P. Yang, D. Lu, X.Z. Fu, R. Sun, C.P. Wong, $NiCo_2O_4$ nanosheets in-situ grown on three dimensional porous Ni film current collectors as integrated electrodes for high-performance supercapacitors, J. Power Sources 286 (2015) 371-379.

81. L. Yu, H. Wu, T. Wu, C. Yuan, Morphology-controlled fabrication of hierarchical mesoporous $NiCo_2O_4$ micro-/nanostructures and their intriguing application in electrochemical capacitors, RSC Adv. 2013, 3, 23709−23714.

82. G. K. Veerasubramani, MSP Sudhakaran, N. R. Alluri, K. Krishnamoorthy, Y. S. Mok, S. J. Kim, Effective use of an idle carbon-deposited catalyst for energy storage applications, J. Mater. Chem. A**,** 4 (2016) 12571-12582.

6. Summary

In this study, we have prepared $NiCo_2O_4$ nanostructures using hydrothermal method as an efficient electrode material for supercapacitor applications. In our first work, we have prepared plate-like $NiCo_2O_4$ nanomaterials. It is found that the $NiCo_2O_4$nanoplates electrode revealed a maximum specific capacitance of 332 F g^{-1} at a scan rate of 5 mV s^{-1}. Furthermore, $NiCo_2O_4$nanoplates electrode exhibited better cycle life with capacitance retention of 86% of the initial capacitance value, even after 2000 cycles. These electrochemical studies suggested that the $NiCo_2O_4$nanoplates area promising electrode material for supercapacitors.

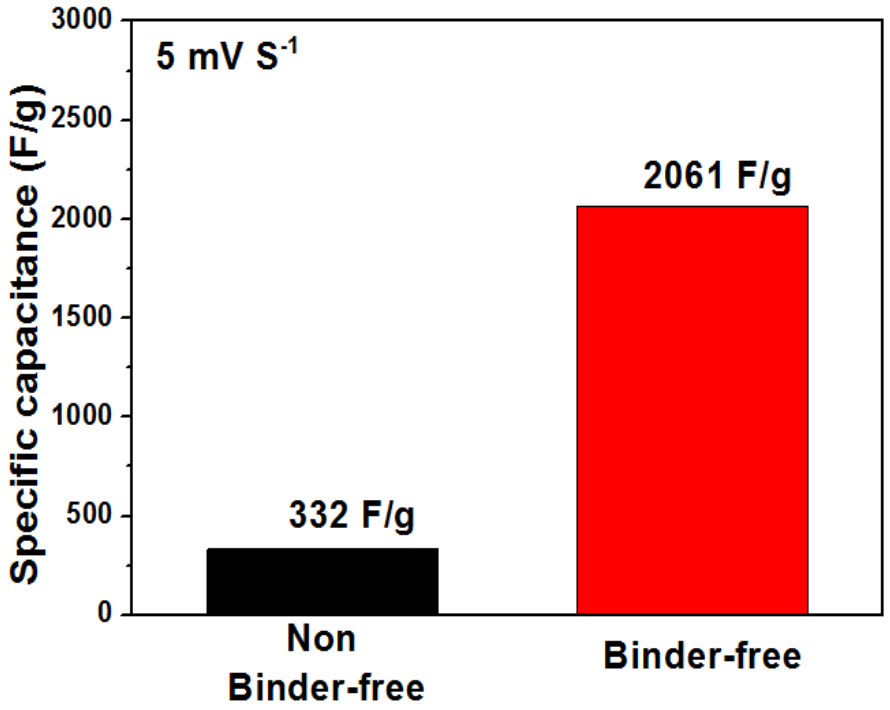

Figure.6.1.1 Comparison of the present work

In second chapter, we have successfully prepared highly porous binder-free $NiCo_2O_4$ nanosheets on Ni foam substrate using a facile hydrothermal method followed by post annealing process. From the morphological analysis, the highly porous nature $NiCo_2O_4$ nanopetals are observed which facilitates the improved surface area for the electrolyte penetration. The electrochemical charge storage behavior of the prepared $NiCo_2O_4$ nanosheets was investigated as a positive electrode for supercapacitor applications. It is noteworthy that the prepared porous binder-free $NiCo_2O_4$on Ni foam electrode exhibited a maximum gravimetric capacitance of 2100 F $g^{-1}$by GCD measurement at the current density of 5 mA cm^{-2} which is almost equal to the capacitance (2061 Fg^{-1}) calculated by CV analysis at the scan rate of 5 mV s^{-1}.Moreover, porous binder-free $NiCo_2O_4$ nanopetals electrode exhibited better durability with capacitance retention of 88.5% of the initial value, even after continuous 2000 cycles. Overall, the obtained electrochemical results suggested that the binder-free $NiCo_2O_4$nanosheets are a promising candidate as a positive electrode material for supercapacitor applications.

Appendix: Publications

1. **T.H. Kim,** G.K. Veerasubramani, S.J. Kim, Synthesis of Hierarchical Porous Flower-like $NiCo_2O_4$ Nanosheets on Ni foam as a Binder-less Electrode for Supercapacitor– **To be submitted**
2. **T.H. Kim**, A. Ramadoss, B. Saravanakumar, G.K. Veerasubramani, S.J. Kim, Applied Surface Science 370, 2016, 452-458. (**I.F: 3.15**)
3. A Ramadoss, **T .H. Kim**, GS Kim, SJ Kim, New Journal of Chemistry 38 (6), 2379-2385. (**I.F : 3.3**)
4. B.Saravanakumar, K.Thiyagarajan, N. R. Alluri, S. SoYoon, **T.H. Kim**, Z.H. Lin, S.-J. Kim, Carbon 84, 2015, 56 – 65. (**I.F : 6.2**)